Novel Modulation Technique

for Radio-over-Fiber Systems

Minhong Zhou

A Thesis

in

The Department

of

Electrical and Computer Engineering

Presented in Partial Fulfillment of the Requirements

for the Degree of Master of Applied Science (Electrical and Computer Engineering) at

Concordia University

Montreal, Quebec, Canada

August, 2007

Your file Votre référence
ISBN: 978-0-494-40900-8
Our file Notre référence
ISBN: 978-0-494-40900-8

Abstract

Novel modulation technique for radio-over-fiber systems

Minhong Zhou

Fiber-optic communications have been widely used and deployed across the globe. As the bottom structure of optical communication networks, optical access networks connect a central office with base stations in local networks. Falling into the category of optical access networks, Radio-over-fiber (RoF) technique offers the future access solutions for high speed and capacity wireless communication. RoF technique uses optical fiber to distribute high frequency RF signals between central office and base stations. At present, two main RoF modulation techniques exist, optical double sideband modulation (ODSB) and optical single sideband modulation (OSSB). OSSB is preferred due to robustness to chromatic dispersion but ODSB not. In typical OSSB, modulation efficiency *i.e.* optical carrier-to-sideband power ratio (OCSR) is merely determined by RF amplitude. Large/small RF signals can lead to small/large OCSR and large/small nonlinear distortions. OCSR directly determines RF output power. The goal of new modulation technique is to improve modulation efficiency by suppressing OCSR and keep nonlinear distortions low.

In this work, we propose and analyze a novel modulation technique, consisting of two parallel dual-electrode Mach-Zehnder modulators (MZMs). With this proposed modulation technique, OSSB with adjustable OCSR can be achieved by adjusting two

DC biases of the MZMs. We first make theoretical analysis and then finish simulation verification. Their results agree with each other very well. Both of them show that RF output power can be greatly improved by adjusting OCSR. Furthermore, the optimum OCSR is 0dB when one RF is applied to modulation optical carrier and it is 3dB in the case of two RF signals.

Acknowledge

I wish to express my sincere appreciation to my supervisor Dr. John Xiupu Zhang for his help and support during my study at Concordia. His insight, expertise and wealth of knowledge are invaluable to me. Without his help, I could not finish this study.

I would like to thank my friends of Li Zhu, Shaofeng An, Chengwei Gu and Xujun Li for their English correction of this thesis.

Finally, I would like to thank my family, especially my girlfriend Quan Zhang, for all the love and support from them.

CONTENTS

List of figures

List of Tables

List of Acronyms and Abbreviations

RoF	Radio over fiber
MZM	Mach-Zehnder modulator
DE-MZM	Dual electrode Mach-Zehnder modulator
OCSR	Optical carrier-to-sideband ratio
MI	Modulation index
IMD	Inter-modulation distortion
HD	Harmonic distortion
IMD3	Third order inter-modulation distortion
SNR	Signal-to-noise ratio
SCM	Sub-carrier modulation
OSSB	Optical single sideband
ODSB	Optical double sideband
QoS	Quality of service
WDM	Wavelength-division-multiplexing
DWDM	Dense-wavelength-division-multiplexing
FDM	Frequency division multiplexing
OTDM	Optical time division multiplexing
RF	Radio frequency
LSB	Lower sideband

USB	Upper sideband
WAN	Wide area network
MAN	Metropolitan area network
LAN	Local area network
PON	Passive optical network
FTTP	Fiber to the premises
FTTH	Fiber to the home
FBG	Fiber Bragg grating
AWG	Arrayed waveguide grating
EMI	Electromagnetic interference
CO	Central office
BS	Base station
IM-DD	Intensity modulation-direct detection
CW	Continuous wave
NF	Noise figure
PD	Photo detector
EDFA	Erbium doped fiber amplifier
SBS	Stimulated Brillouin scattering

List of mathematical symbols

r	Power division ratio of upper path to lower path in a single DE-MZM
ER	Extinction ratio
V_π	Voltage inducing π phase shift in DE-MZM
ξ	Modulation index
ξ_1	Normalized bias $1DC_{OP}$
ξ_2	Normalized bias $2DC_{OP}$
t_{ff}	Insertion loss of DE-MZM
ω	Angular frequency of RF signal
θ	Initial phase of RF signal
E_0	Intensity of incident light wave from CW laser
E_1	Intensity of modulated light wave along path1
E_2	Intensity of modulated light wave along path2
E_3	Intensity of modulated light wave along path3
E_4	Intensity of modulated light wave along path4
E_{out}	Intensity of modulated light wave after the proposed modulator
$J_n(z)$	N_{th} order Bessel function
$\Re$	Responsivity of PD
G_{EDFA}	Gain of EDFA

Chapter 1 Introduction

1.1 Fiber-optic communication

Driven by the increasing demand of internet data traffic, fiber-optic communication system has been developed dramatically and the optical transmission links have been widely built all over the world. The fiber communication system offers a network infrastructure of huge information capacity and has already become the essential part of the whole communication network. The fiber system delivers both the voice-oriented and the data-oriented information in a very economical way, while achieving the required quality of service (QoS).

As the crucial element of an optical signal transmission, optical fibers offer wider available bandwidth, lower signal attenuation, and smaller signal distortion than other sorts of wired physical media. The optical fiber can allow long transmission distance at high bit rates. Fig. 1.1 shows a typical attenuation curve of a single-mode optical fiber used today. It pictures out the relationship between the transmission attenuation loss and the available bandwidth. As can be seen in Fig. 1.1, the transmission attenuation is relatively low when the wavelength of fiber is about 1310 nm and 1550 nm. For instance, at the wavelength of 1550 nm, the fiber attenuation loss is 0.2 dB/km, which is suitable. Normally, the usable optical wavelength can be split into several wavelength bands. The bands around the minimum attenuation region usually is referred to C and L bands, have

been considered as the most suitable ones for high channel count DWDM transmission, and have been already widely used for transmission purposes. The C band occupies wavelength approximately from 1530 to 1560 nm, while the L band includes wavelengths between 1580 and 1610 nm. The S covers shorter wavelengths usually above 1460 nm, where the optical fiber attenuation is slightly higher than in the C and L bands.

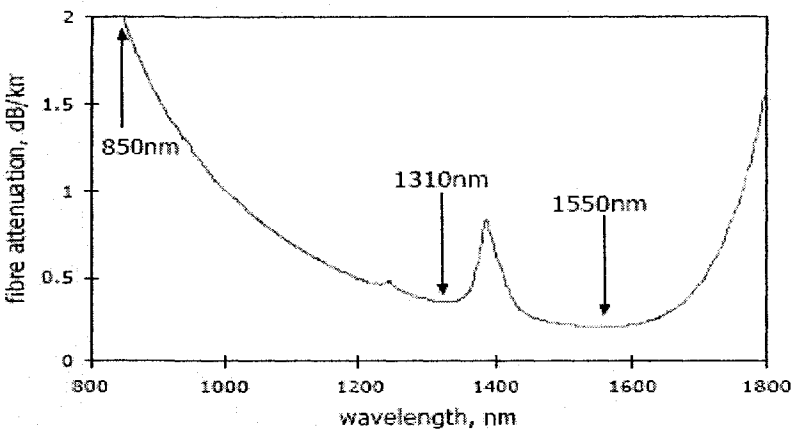

Fig. 1.1 Transmission attenuation losses versus wavelength

The deployment of the wavelength division multiplex (WDM) technology is the foundation for optical networks. The use of WDM over the same fiber provides a simple way for extending the system capacity to beyond 1 Tb/s. WDM corresponds to the scheme in which multiple optical carriers at different wavelengths are modulated by using independent electrical bit streams (which may themselves use time-division multiplexing and frequency-division multiplexing techniques in the electrical domain) and are then transmitted over the same fiber. The optical signal at the receiver is de-multiplexed into separate channels by using an optical technique. WDM has the potential for exploiting the large bandwidth offered by optical fibers. For example,

hundreds of 10 GB/s channels can be transmitted over the same fiber when channel spacing is reduced to below 100GHz.

The optical network structure can be represented by three concentric circles as shown in Fig. 1.2.

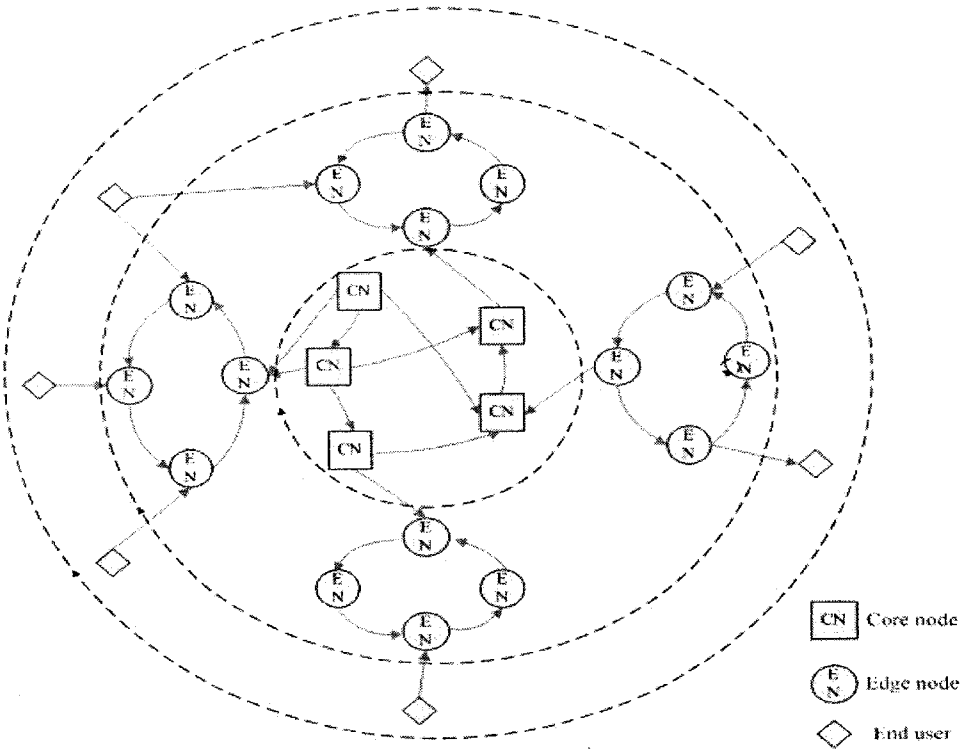

Fig. 1.2 Optical network structure

The central part of this structure is a long-haul core network interconnecting big cities or major communication hubs. The connections between big cities on different continents have been made by using submarine optical transmission systems. The core network is a generic name, but very often it can be recognized as wide area network (WAN). The second part of the optical network structure is edge optical network, which is deployed within a smaller geographical area (usually in a metropolitan area or even smaller geographic region). The edge network is often recognized as a metropolitan area network

(MAN). Finally, the access network is a peripheral part of the optical network related to the last-mile access and bandwidth distribution to the individual end users (corporate, government, medical, entertainment, scientific, and private). Access networks examples include the enterprise local area networks (LAN) and a distribution network that connects the central office location with individual users. Compared with the progress made in the first two structures, the optical access technology is not mature and people still can develop a lot. Basically, all of the efforts concerning researching optical access networking focus on RoF (radio over fiber) and PON (passive optical network). RoF mainly offers the future wireless access solution in which the radio frequency signals propagate over the fiber. The main advantages of this technology are that it can make the base stations or antenna stations (the corresponding definition to central office) simpler so to simplify the installation and maintenance and can offer much wider bandwidth with lower attenuation loss so to facilitate higher quality mobile communication service than the conventional. The thesis proposes and develops a new modulation technique for RoF and more details concerning RoF will be presented in the following section. Passive Optical Networks (PON) is the leading technology being used in FTTP (Fiber to the Premises), FTTH (Fiber to the Home) deployments. The advantages of PON over the conventional technique are that it can offer much wider bandwidth with deeper penetration and it needs less fiber deployment with only one port in central office.

1.2 Radio over fiber (RoF)

As a promising access technique, RoF can be applied in cellular networks, satellite communications, video distribution systems, wireless LANs, vehicle communication and control, phase array radar etc. Applications for RoF in cellular networks are usually split into three types: radio coverage extension and capacity distribution and allocation. The first case includes applications for railway and motorway tunnels, canyons, and similar dead spot areas that because of their specific needs often do not justify the costs of installing and operation new BS. The second case includes applications for subway stations, exhibition grounds, airports, downtown street levels, and other densely populated environments where the traffic requirement leads to dedicated radio channels that need to be distributed appropriately. Both of the preceding two cases have been practically implemented in the existing cellular networks. The third cases will be applicable for the future 3G or 4G communication networks. As cell size of the future cellular network decreases and frequency of RF signal increases, RoF offers the great access solution to the future cellular communication networks.

1.2.1 What is RoF

Due to their ease of installation in comparison to fixed networks, wireless communication has experienced tremendous growth in the last decade. However, as the demand of high quality service like high definition video talk, internet data transferring

increases considerably, the capacity of the current narrowband wireless access networks seems insufficient.

One natural way to increase capacity of wireless communication systems is to deploy smaller cells (micro- and pico-cells) [1] [2]. This is generally difficult to achieve at low-frequency microwave carriers, but by reducing the radiated power at the antenna, the cell size may be reduced somewhat. Pico-cells are also easier to form inside buildings, where the high losses induced by the building walls help to limit the cell size. Smaller cell sizes lead to improved spectral efficiency through increased frequency reuse. But, at the same time, smaller cell sizes mean that large numbers of base stations are needed in order to achieve the wide coverage required for ubiquitous communication systems. Furthermore, extensive feeder networks are needed to service the large number of base stations. Therefore, unless the cost of the base stations and the feeder network are significantly low, the system-wide installation and maintenance costs of such systems would be rendered prohibitively high. This is where Radio-over-Fiber (RoF) technology comes in. It achieves the simplification of the base stations through consolidation of radio system functionalities at a centralized head end, which are then shared by multiple base stations.

Another way to increase the capacity of wireless communication systems is to increase the carrier frequencies. Higher carrier frequencies offer greater modulation bandwidth, but may lead to increased costs of radio front-ends in the base stations. In conventional wireless communication systems, the media for transmission channel is the air. However,

radio signals with high frequencies will attenuate greatly when propagating in the air. Even the penetration ability of going through obstacles into building will also decrease extremely. When radio signals at the frequency of 60 GHz propagate in the air, the attenuation loss can be as large as 10-15 dB/km. In other words, if we transmit typical radio signal at 60 GHz directly over the air, it will only be able to propagate for less than 2 km.

Radio-over-Fiber (RoF) technique entails the use of optical fiber links to distribute radio frequency (RF) signals from a central office to base stations. In narrowband communication systems, RF signal processing functions such as frequency up-conversion, carrier modulation, and multiplexing, are performed at the base stations, and immediately fed into the antenna. RoF makes it possible to centralize the RF signal processing functions in one shared location (Central Office), and then to use optical fiber, which offers low signal loss (0.2 dB/km for 1550 nm, and 0.5 dB/km for 1310 nm wavelengths) to distribute the RF signals to the base stations. By so doing, base stations are simplified significantly, as they only need to perform optoelectronic conversion and amplification functions. The centralization of RF signal processing functions enables equipment sharing, dynamic allocation of resources, and simplified system operation and maintenance. These benefits can translate into major system installation and operational savings [3], especially in wide-coverage broadband wireless communication systems, where a high density of base stations is necessary as discussed above.

1.2.2 Benefits of RoF technique

Some of the advantages and benefits of the RoF technology compared with electronic signal distribution are given below.

a. Low attenuation loss

Commercially available standard Single Mode Fibers (SMFs) made from glass (silica) have attenuation losses below 0.2 dB/km and 0.5 dB/km in the 1550 nm and the 1310 nm windows, respectively. We have mentioned the situation of RoF over the air above. Obviously, it is not suitable for being the transmission medium when RF signals' frequencies increase greatly. As another common type of transmission medium, coaxial cables' losses are higher by three orders of magnitude at higher frequencies. For instance, the attenuation of a ½ inch coaxial cable (RG-214) is >500 dB/km for frequencies above 5 GHz [4]. Therefore, by transmitting microwaves in the optical form, transmission distances are increased several folds and the required transmission powers reduced greatly.

b. Large bandwidth

Optical fibers offer enormous bandwidth. There are three main transmission windows, which offer low attenuation, namely the 850 nm, 1310 nm, and 1550 nm wavelengths. For a single SMF optical fiber, the combined bandwidth of the three windows is in the excess of 50 THz. However, today's state-of-the-art commercial systems utilize only a fraction of this capacity (1.6 THz). But developments to exploit more optical capacity per

single fiber are still continuing. The main driving factors towards unlocking more and more bandwidth out of the optical fiber include the availability of low dispersion (or dispersion shifted) fiber, the Erbium Doped Fiber Amplifier (EDFA) for the 1550 nm window, and the use of advanced multiplex techniques namely Optical Time Division Multiplexing (OTDM) in combination with Dense Wavelength Division Multiplexing (DWDM) techniques. The enormous bandwidth offered by optical fibers has other benefits apart from the high capacity for transmitting microwave signals. The high optical bandwidth enables high speed signal processing that may be more difficult or impossible to do in electronic systems. In other words, some of the demanding microwave functions such as filtering, mixing, up- and down-conversion, can be implemented in the optical domain [5]. For instance, mm-wave filtering can be achieved by first converting the electrical signal to be filtered into an optical signal, then performing the filtering by using optical components such as the Mach Zehnder Interferometer (MZI) or Fiber Bragg Gratings (FBG), and then converting the filtered signal back into electrical form. Furthermore, processing in the optical domain makes it possible to use cheaper low bandwidth optical components such as laser diodes and modulators, and still be able to handle high bandwidth signals [6]. The utilization of the enormous bandwidth offered by optical fibers is severely hampered by the limitation in bandwidth of electronic systems, which are the primary sources and receivers of transmission data. This problem is referred to as the "*electronic bottleneck*". The solution around the electronic bottleneck lies in effective multiplexing. OTDM and DWDM techniques mentioned above are used

in digital optical systems. In analogue optical systems including RoF technology, Sub-Carrier Multiplexing (SCM) is used to increase optical fiber bandwidth utilization. In SCM, several microwave sub carriers, which are modulated with digital or analogue data, are combined and used to modulate the optical signal, which is then carried on a single fiber [7], [8]. This makes RoF systems cost-effective.

c. Immunity to radio frequency interference

Immunity to Electromagnetic Interference (EMI) is a very attractive property of optical fiber communications, especially for microwave transmission. This is so because signals are transmitted in the form of light through the fiber. Because of this immunity, fiber cables are preferred even for short connections at mm-waves. Related to EMI immunity is the immunity to eavesdropping, which is an important characteristic of optical fiber communications, as it provides privacy and security.

d. Easy installation and maintenance

In RoF systems, complex and expensive equipment is kept in central office, thereby making the BSs simpler. For instance, most RoF techniques eliminate the need for a LO and related equipment at the BSs. In such cases a photo detector, an RF amplifier, and an antenna make up the BS. Modulation and switching equipment is kept in the central office and is shared by several BSs. This arrangement leads to smaller and lighter BSs, effectively reducing system installation and maintenance costs. Easy installation and low maintenance costs of BSs are very important requirements for mm-wave systems, because of the large numbers of the required BSs.

e. Reduced power consumption

Reduced power consumption is a consequence of having simple BSs with reduced equipment. Most of the complex equipment is kept in the central office. In some applications, the BSs are operated in passive mode. For instance, some 5 GHz Fiber-Radio systems employing pico-cells can have the BSs operate in passive mode [9]. Reduced power consumption at the RAU is significant considering that BSs are sometimes placed in remote locations not fed by the power grid.

f. Dynamic resource allocation

Since the switching, modulation, and other RF functions are performed at a central office, it is possible to allocate capacity dynamically. For instance in a RoF distribution system for GSM traffic, more capacity can be allocated to an area (e.g. shopping mall) during peak times and then re-allocated to other areas when off-peak (e.g. to populated residential areas in the evenings). This can be achieved by allocating optical wavelengths through Wavelength Division Multiplexing (WDM) as need arises [10]. Allocating capacity dynamically as need for it arises obviates the requirement for allocating permanent capacity, which would be a waste of resources in cases where traffic loads vary frequently and by large margins [3]. Furthermore, having the central office facilitates the consolidation of other signal processing functions such as mobility functions, and macro diversity transmission [10].

1.2.3 Techniques for generating and transporting RF signals over optical fiber

There are several optical techniques for generating and transporting microwave signals over fiber. RoF techniques may be classified in terms of the underlying modulation/detection principles employed. In that case, the techniques may be grouped into three categories, namely Intensity Modulation- Direct Detection (IM-DD), Remote Heterodyne Detection (RHD) [11], and harmonic up-conversion techniques. IM-DD is the simplest method and also the most widely used at present. Not only the modulation techniques discussed below but also our modulation technique belongs to this category. SCM is another principal technique which is used extremely widely in RoF systems. This technique can help RoF make full use of the sufficiency optical fiber bandwidth.

a. Some techniques for generating RF signals over optical fiber

IM-DD is simply to directly modulate the intensity of the light source with the RF signal itself and then to use direct detection at the photo detector to recover the RF signal. There are two ways of modulating the light source. One way is to let the RF signal directly modulate the laser diode's current. The second option is to operate the laser in continuous wave (CW) mode and then use an external modulator such as the Mach-Zehnder Modulator (MZM), to modulate the intensity of the light. The two options are shown in Fig.1.3. In both cases, the modulating signal is the actual RF signal to be distributed. The RF signal must be appropriately pre-modulated with data prior to

transmission.

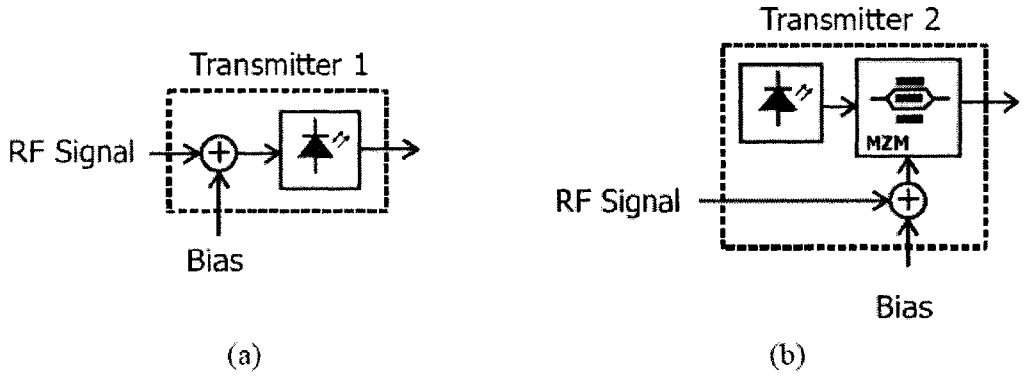

Fig. 1.3 Generating RF signals by direct intensity modulation (a) of a laser; (b) using an external modulator

Evidently, direct intensity modulation is, in principle, even simpler than external modulation. So it is used everywhere that it can be used. One limiting phenomenon to its use is the modulation bandwidth of the laser. Relatively simple lasers can be modulated to frequencies of several giga-hertz, say 5-10 GHz. That is why at higher microwave frequencies, say, above 10 GHz, external modulation rather than direct modulation is applied.

b. Subcarrier modulation in RoF systems

Subcarrier Modulation (SCM) is a maturing, simple and cost effective approach for exploiting optical fiber bandwidth in analogue optical communication systems in general and in RoF systems in particular. In SCM, multiple RF signals (the sub-carriers) is used to modulate an optical carrier at the transmitter's side. In this thesis, maximally two sub-carriers are multiplexed to help us to investigate how SCM influences the system's performance. Fig. 1.4 illustrates what SCM is.

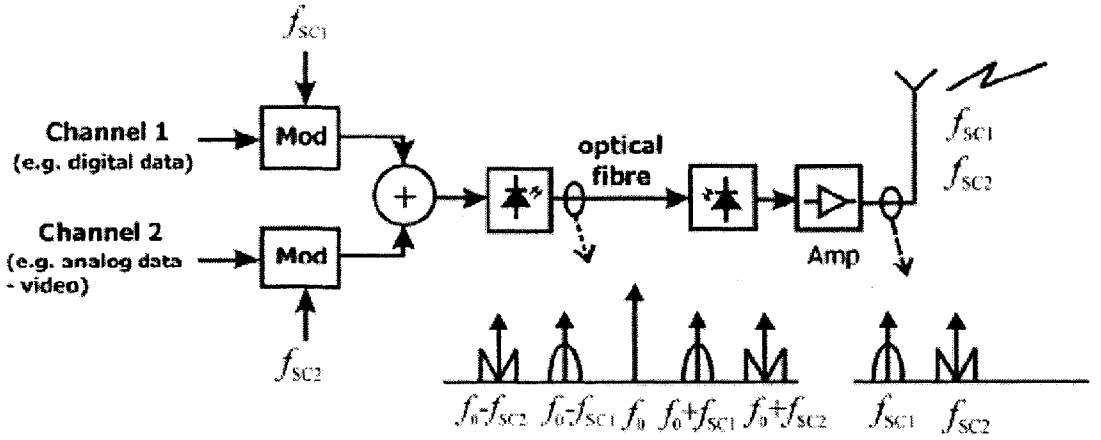

Fig. 1.4 Sub-carrier modulation of mixed digital and analogue signals

To multiplex multiple channels to one optical carrier, multiple sub-carriers are first combined and then used to modulate the optical carrier as shown in Fig. 1.4. At the receiver's side the sub-carriers are recovered through direct detection and then radiated. Different modulation schemes may be used on separate sub-carriers. One sub-carrier may carry digital data, while another may be modulated with an analogue signal such as video or telephone traffic. In this way, SCM supports the multiplexing of various kinds of mixed mode broadband data. Modulation of the optical carrier may be achieved by either directly modulating the laser, or by using external modulators such as the MZM.

1.2.4 Limitations of RoF technique

Since RoF involves analogue modulation, and detection of light, it is fundamentally an analogue transmission system. Therefore, signal impairments such as noise and distortion, which are important in analogue communication systems, are important in RoF systems as well. These impairments tend to limit the receiver's sensibility and Noise Figure (NF)

of the RoF links.

Although there are a lot of sources of interference like shot noise, thermal noise, chromatic dispersion, nonlinear distortion due to analogue nonlinear modulation is the dominant among all the harmful factors. Let's take an example for the systems in which MZM is used. MZM has a squared cosine transfer function in power. In other word, it has a nonlinear transfer function. When RF signals are applied to modulate the optical carrier in MZM, nonlinear distortions including harmonics distortions (HDs) and inter-modulation distortions (IMDs) will generate. Basically, HDs mainly depends on MI. The increase of MI will lead to that the modulation will happen in the region with more serious nonlinearity so the intensities of HDs will become larger and larger. Concerning IMDs, it is principally determined by MI and the number of RF carriers. As MI increases, the intensities of IMDs also will become more and more serious. Every RF sub-carrier can inter-modulate with each other. Therefore, as multiple like two or more RF sub-carriers are used to modulate the optical carrier, this can cause more happening of IMDs.

Theoretically, there will be unlimited number of high order optical spectrum components including HDs and IMDs after light wave modulated by RF signals. Due to the limited bandwidth of the optical equipments like Multiplexer, EDFA, Photodetector, etc, the high order like larger than three optical spectrum components will be filtered out by those optical equipments. Therefore, those low order nonlinear distortions make great contribution to degrade the system's performance. Compared with other low order

nonlinear distortions, the third order IMDs (IM3) is the most difficult to be filtered out by optical filters because they are very close to the fundamental spectrum component. IM3 may bring devastating impact on the receiver's sensitivity if we can't handle this very well.

1.3 Literature review and motivation

At present, the most commonly used modulation schemes in the external intensity modulation category are optical double sideband modulation (ODSB) and optical single sideband modulation (OSSB). Generally, ODSB can be realized by employing MZM. In an ODSB system, the transmission and distribution of the millimeter-wave radio signal to and from base stations (BS) is susceptible to chromatic dispersion, which seriously degrades the transmission distance [12]-[14]. Contrastly, by using OSSB scheme, the degradation of the transmission distance can be effectively restrained [15]-[18]. Typical OSSB is generated by employing a dual-electrode Mach-Zehnder modulator (DE-MZM) [19]. When we choose the millimeter RF signal of large amplitude to modulate the optical carrier in DE-MZM, considerable harmful nonlinear distortions, *i.e.* HDs and IMDs, will be generated in the system due to the analogue modulation process of DE-MZM. However, when we choose the millimeter RF signals of small amplitude to modulate the optical carrier, very low modulation efficiency will be produced [15]. For instance, the power of the optically modulated millimeter wave sideband can be over 20 dB lower than that of the optical carrier. To improve the performance of RoF transmission and signal

processing systems, the optical power of mm-wave are increased by starting with the high power light sources and utilizing the optical amplifiers [21]. However, these methods also increase the average optical power to the photo detector (PD) simultaneously. The high power on high-frequency PD's can cause the harmonic distortion, the response reduction, and the damage to the receiver due to the extremely large optical power incident on the optical detector [19] [20] [21]. Besides, the low modulation efficiency also causes the waste of the system resource. The optical power of mm-wave sideband is still much lower than that of optical carrier, which means the optical signal power transmitted from modulator contains a limited portion of RF sideband with useful information but a huge portion of optical carrier with no information.

So far, suppressing the main optical carrier has become a popular way to improve the modulation efficiency. Lots of techniques concerned have been proposed and demonstrated, *e.g.* Brillouin [22], external optical filtering [19] [20] [21] and optical attenuation [23]. However, all these techniques have one common disadvantage, which is the increasing complexity of RoF system. In [22], the author mainly made use of Stimulated Brillouin Scattering (SBS) mechanism in which an optical pump was necessary to realize the SBS. External optical filters are the components to remove the excessive power of optical carriers [19] [20]. In [21], Fiber Bragg Grating (FBG) acts like an external filter and its values of reflectivity are adjusted to determine the degree of suppressing optical carrier. In [23], arrayed waveguide grating (AWG) is utilized to attenuate the optical carrier. Besides the complexity and inconvenience caused by extra

optical or electrical components, other harmful factors also degrade the performance of the RoF system. In the case of SBS, the process was relatively unstable and noisy [22]. Concerning the external optical filter, it may introduce distortions into the RF signal [22]. Thus all of the techniques mentioned above are not perfectly effective for suppressing the main optical carrier. Recently, a distinct way to suppress the optical carrier is proposed by using a low biased MZM [24]. This method suppresses the optical carrier enormously by adjusting DC bias and is effective to obtain a large range of optical carrier-to-sideband ratio (OCSR) without utilizing other optical or electrical components, where OCSR of an optically modulated mm-wave signal is defined as the ratio of the power of optical carrier to that of the first-order sideband. Nevertheless, the disadvantage of this technique is that the format of modulated optical signal is ODSB, which is extremely vulnerable to chromatic dispersion degrading the performance of RoF system considerably.

In order to overcome the disadvantage referred above, we get a good motivation to develop and investigate a new modulation technique, in which OCSR should be adjustable conveniently and OSSB optical signal should be generated to conquer the chromatic dispersion simultaneously. Furthermore, the optimum OCSR for maximizing the transmission performance in fiber-radio link is 0 dB when one RF signal is used to modulate optical carrier. Therefore, not only making the OCSR adjustable, we also plan to realize the optimum OCSR in our modulation technique. In [21], the analysis of the optimum OCSR with one RF signal has been presented. In this thesis, we investigate the optimum value of the OCSR when applying two RF signals. Two RF signals

inter-modulate with each other while the signals are modulating the optical carrier. The investigation is also made to show how our modulation technique affects the third order inter-modulation (IM3), which is most detrimental nonlinear distortion to the performance of system.

1.4 Organization of the thesis

Chapter 1 is the introduction and background section. The basic theories of optical communication and radio-over-fiber are presented. A detailed review of current modulation techniques is also given in this chapter.

In Chapter 2, a novel modulation technique to improve the performance of the system is proposed and the principle is explained. Some parameters, which are crucial to the new modulation technique, are analyzed in detail. We also establish the analytical model of the system in which the new modulation technique is applied. Several key criteria to evaluate the performance of system are quantified by accurate expressions.

In Chapter 3, some simulations are presented to verify the theory of the proposed modulation technique.

Chapter 4 describes the conclusions and future work.

Chapter 2 Proposed modulation technique and theoretical analysis

In this chapter, our modulation technique is proposed and the theoretical analysis is also presented. The goal of our proposed technique is to improve the modulation efficiency which is the crucial parameter to influence the performance of fiber-radio link. Intuitively, the goal is illustrated in Fig. 2.1.

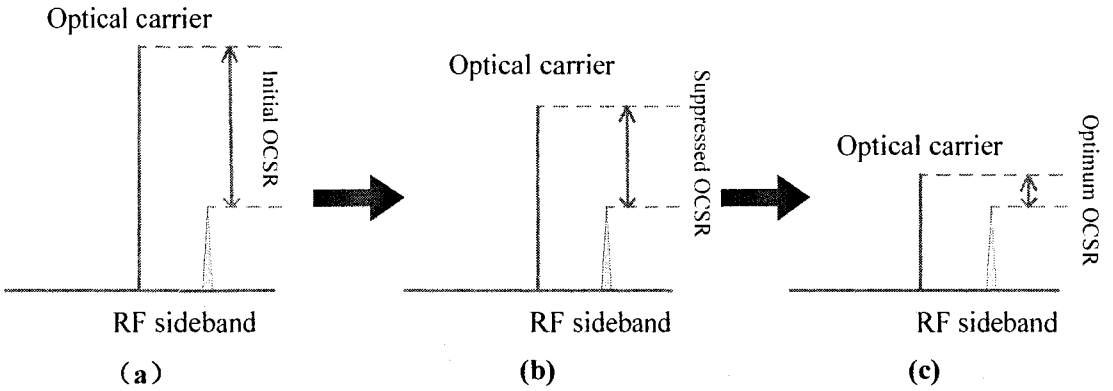

Fig. 2.1 Schematic of improving modulation efficiency

Fig. 2.1 schematically shows how modulation efficiency is improved by suppressing optical carrier. Fig. 2.1 (a) represents the relative positions of the optical carrier and the RF sideband before the optical carrier gets suppressed. It is obvious that the OCSR is tremendously large and the modulation efficiency is considerably low. Fig. 2.1 (b) displays the situation after the optical carrier is suppressed to a certain extent, where the OCSR is decreased by a certain obvious level and the modulation efficiency is highly improved. Fig. 2.1 (c) exhibits the optimum OCSR after the optical carrier is further suppressed. The optimum OCSR in Fig. 2.1 (c) doesn't indicate the actual value of the

optimum OCSR, which practically may be smaller or larger. For instance, the optimum OCSR in [21] is 0 dB. However, all the investigation was developed in the situation of one RF signal. In this thesis, we investigate whether the optimum OCSR, 0 dB, can be realized by employing our modulation technique. Furthermore, we also make effort to find out the optimum OCSR in the situation of two RF signals.

2.1 Principle of proposed modulation technique

In our modulation technique, dual electrode Mach-Zehnder modulator (DE-MZM) is one of the vital components. It is fabricated by $LiNbO_3$ material. Two Titanium-diffused $LiNbO_3$ waveguides form two paths of a MZM interferometer. The refractive index of $LiNbO_3$ can be changed by applying an external voltage. That implies when light waves go through the paths, their phase will be shifted by the value determined by the refractive index. If the external voltage is from a DC bias, the phase of light wave will be shifted by a constant. If the external voltage is from a RF signal, the phase of light wave will vary according to the amplitude changing of RF signal. After running through the respective waveguides, the two paths of optical signals are combined together to interfere with each other. The final optical signal after interference depends on the phases of the optical signals from two paths. For instance, in the absence of external voltage, the optical fields in the two paths of the MZM interferometer experience identical phase shift and interfere constructively. The additional phase shift introduced in one of the arms through voltage-induced index changes destroys the constructive nature of the interference and

reduce the transmitted intensity.

When one RF signal is applied to modulate optical carrier, the principle of the modulation process is illustrated in Fig. 2.2.

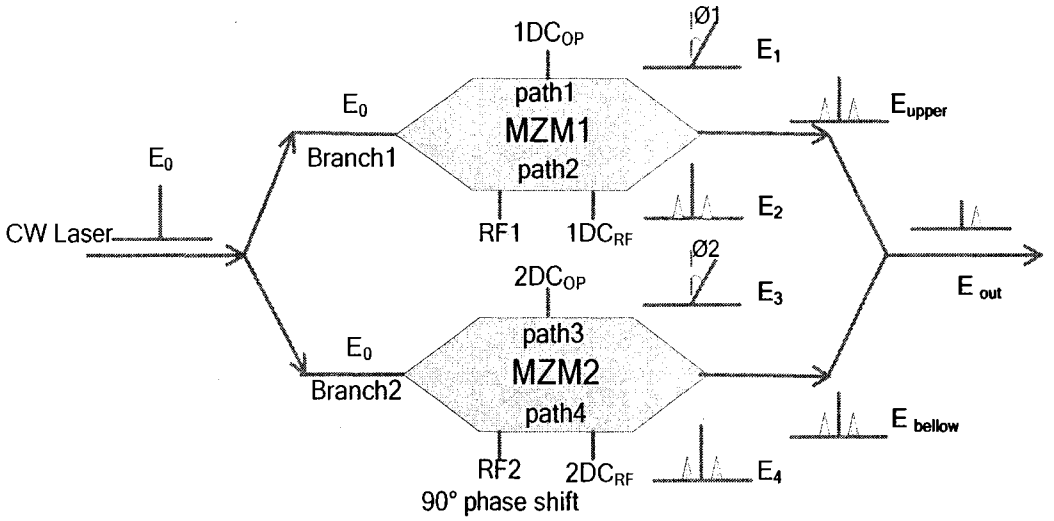

Fig. 2.2 Schematic of our proposed modulation technique (one sub-carrier)

From the left side to right side in Fig. 2.2, the light wave from laser is equally split into two branches. The upper one is identified as Branch1 while the lower one is named by Branch2. Then, the optical carriers in the two branches are coupled into two DE-MZMs, the essential components of our modulation technique. The DE-MZM along Branch1 is identified as MZM1 while the one associated with Branch2 is named by MZM2. Inside each MZM two paths, upper one and lower one, are designed. The upper ones of MZM1 and MZM2 are named by path1 and path3 separately. The lower ones of MZM1 and MZM2 are identified as path2 and path4. Three inputs are connected onto each MZM, thus for the parallel DE-MZMs, six inputs with the name of RF_1, RF_2, $1DC_{RF}$, $2DC_{RF}$, $1DC_{OP}$ and 2 DC_{OP} are designed. Consequently, six inputs are grouped into three pairs, *i.e.*

RF pair, DC_{RF} pair, and DC_{OP} pair. The RF pair consisting of RF_1 and RF_2 is reserved for the input RF signals, which have a 90^{o} phase discrepancy. The DC_{RF} pair consisting of $1DC_{RF}$ and $2DC_{RF}$ is connected to two DC biases which are set to the quadrature point. The DC_{OP} pair consisting of $1DC_{OP}$ and $2DC_{OP}$ is for two other DC biases, whose values need to be critically evaluated for the optimal OCSR and the optimum effect of modulation.

As introduced above, the light wave from CW laser is equally split into Branche1 and Branch2, and then respectively coupled into MZM1 and MZM2 at the same time, which means that the optical carrier is split into Path1, Path2, Path3 and Path4. The intensities of the light wave along Branch1 and Branch2 are identical; however, after the light wave gets into the different paths of MZMs, the intensities along Path1, Path2, Path3 and Path4 are different due to the extinction ratio. The extinction ratio is one of the core parameters of MZM, which represents the difference between the upper path and lower path power split ratio. An ideal MZM has an infinite extinction ratio, though this is not realistic in industry. After modulated by two DC biases DC_{OP}, the two optical carriers coupled into Path1 and Path3 are phase shifted by two independent constant values which are determined by the values of $1DC_{OP}$ and $2DC_{OP}$ respectively. Along Path2 and Path4 driven by RF signals and the other DC biases DC_{RF}, not only the phases the optical carriers are shifted but also two RF sidebands (upper RF sideband and lower RF sideband) are generated next to the optical carrier in each optical signal. The inputs of RF pair and DC_{RF} determine the amplitudes and the phases of both optical carrier and RF sidebands.

When the outputs from the four paths are combined together, the optical carriers from different paths will interfere with each other and their individual phases determine the final intensity of the optical carrier. Besides that, the upper RF sideband from Path2 will interfere with that from Path4 and similarly the lower RF sideband from Path2 will also interfere with that from Path4. The result of RF sideband interference also depends on their individual phases. If we set the DC_{RF} pair at quadrature point, either the upper RF sideband or the lower RF sideband from Path2 will have the opposite phase against that from Path4. In that case, either the upper RF sideband or the lower RF sideband will be canceled. As for whether the upper one or the lower one is canceled, it depends on which original RF signal is associated with the high biasing point. In another words, if one of DC_{RF} which locates in the same DE-MZM with the original RF signal is biased at $\frac{V_\pi}{2}$, lower sideband will be eliminated. Reversely, it is also correct. In all, we can choose the proper inputs for RF pair and DC_{RF} pair to realize OSSB at first and can also adjust the power level of the optical carrier by sweeping the values of DC_{OP}. If we desire to suppress optical carrier to obtain a certain OCSR, the appropriate biasing points of DC_{OP} need to be decided.

When two RF signals are used to modulate optical carrier, both of the two signals are phase shifted by 90^o. The original signals are combined together to be applied onto RF_1 and the shifted signals onto RF_2. The principle of the modulation process is illustrated as Fig. 2.3.

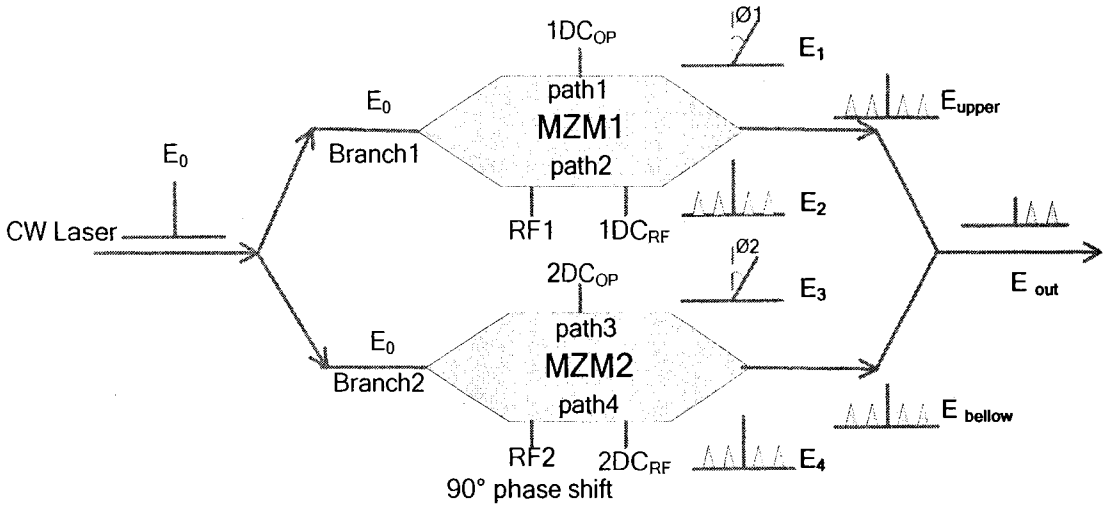

Fig. 2.3 Schematic of our proposed modulation technique (two sub-carriers)

Comparing Fig. 2.3 with Fig. 2.2, we can make conclusion that the principles are almost the same except the number of sidebands. In Fig. 2.3, along both Path2 and Path4 totally four RF sidebands exist, which are two upper RF sidebands and two lower RF sidebands. The processes of suppressing optical carrier and canceling either upper sidebands or lower sidebands are the same as above. In the optical spectrum of the final output E_{out}, either two upper RF sidebands or two lower RF sidebands appear. In the thesis, the amplitudes of the two RF signals are chosen equivalent to each other so the power intensities of RF_1 sidebands are identical to those of RF_2 sidebands. Therefore, OCSR for both RF signals are equivalent and we merely need one mathematical expression to develop the analysis with reference to OCSR.

2.2 Theoretical analysis of proposed modulation technique

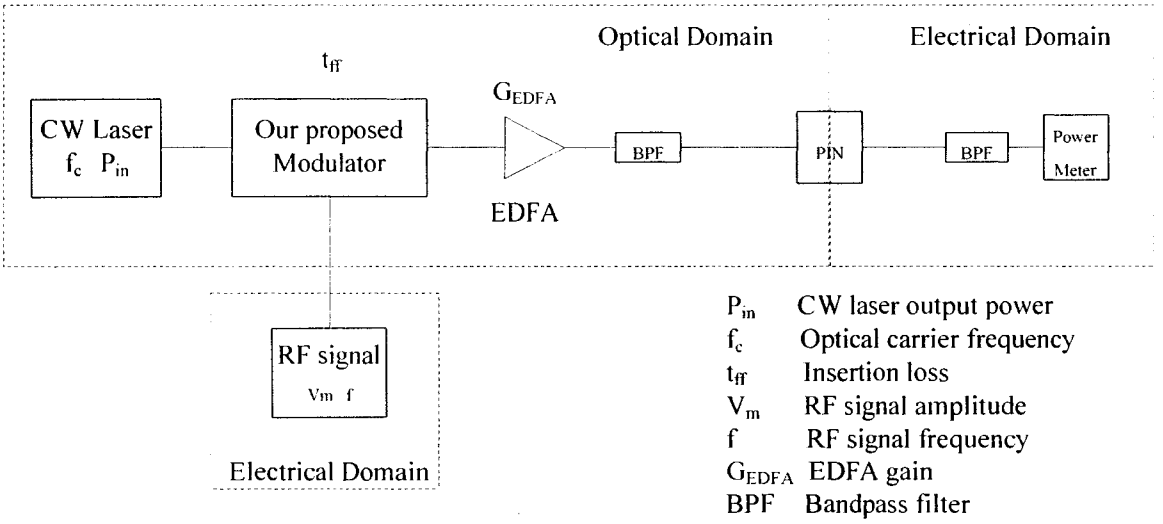

Fig. 2.4 Schematic of the analytical model

Fig. 2.4 shows the schematic diagram of the analytical model to evaluate the performance in a millimeter-wave fiber-radio link incorporating our modulation technique. The CW laser is modeled as a single mode source of frequency f_c and optical field amplitude of E_0. The principle and configuration of our proposed modulation technique is interpreted from above.

2.2.1 Proposed modulator driven by one RF signal

We first investigate the situation in which one optical carrier carries one sub-carrier. Here, $1DC_{RF}$ and $2DC_{RF}$ are set to 0 V and $\frac{V_\pi}{2}$ respectively. The amplitudes of the modulated light waves along Path1, Path2, Path3 and Path4 are E_1, E_2, E_3 and E_4 respectively, which are represented as follows

$$E_1 = \frac{\sqrt{t_{ff}}}{2} E_0 e^{i\frac{V_{DC1}}{V_\pi}\pi}$$

$$E_2 = r\frac{\sqrt{t_{ff}}}{2} E_0 e^{-i\frac{V_1}{V_\pi}\pi}$$

$$E_3 = \frac{\sqrt{t_{ff}}}{2} E_0 e^{i\frac{V_{DC2}}{V_\pi}\pi}$$

$$E_4 = r\frac{\sqrt{t_{ff}}}{2} E_0 e^{-i\left(\frac{V_2}{V_\pi}+\frac{1}{2}\right)\pi}$$

where t_{ff} is the insertion loss of MZM and E_0 is the intensity of the incident light wave from CW laser. r is the power division ratio of upper path to lower path in a single DE-MZM and depends on Extinction Ratio $ER = \left(\frac{1+r}{1-r}\right)^2$. V_{DC1} and V_{DC2} are the DC biases applied on $1DC_{OP}$ and $2DC_{OP}$. V_π is the voltage which can induce π phase shift in DE-MZM. V_1 and V_2 represent the inputs of RF signals as follows

$$V_1 = V_m cos(\omega t + \theta) \tag{1}$$

$$V_2 = V_m cos\left(\omega t + \theta - \frac{\pi}{2}\right) \tag{2}$$

where V_m, ω and θ are the input RF signal's amplitude, angular frequency and initial phase respectively. We define normalized DE-MZM bias parameters as: $\xi = \frac{V_m}{V_\pi}$,

$\xi_1 = \frac{V_{DC1}}{V_\pi}$, $\xi_2 = \frac{V_{DC2}}{V_\pi}$.

After combining all the four paths together, we get E_{out}

$$E_{out}(t) = \frac{\sqrt{t_{ff}}}{2} E_0 \left[e^{i\xi_1\pi} + e^{i\xi_2\pi} + re^{-i\xi\pi\cos(\omega t+\theta)} + re^{-i\frac{\pi}{2}} e^{-i\xi\pi\cos\left(\omega t+\theta-\frac{\pi}{2}\right)} \right] \tag{3}$$

According to Bessel function $e^{iz\cos\varphi} = \sum_{n=-\infty}^{\infty} i^n J_n(z) e^{in\varphi}$, we can expand it as follows

$$E_{out}(t) = \frac{\sqrt{t_{ff}}}{2} E_0 \left\{ e^{i\xi_1\pi} + e^{i\xi_2\pi} + r \sum_{n=-\infty}^{\infty} \left[i^n J_n(\xi\pi) e^{in(\omega t+\theta+\pi)} - i^{n+1} J_n(\xi\pi) e^{in\left(\omega t+\theta+\frac{\pi}{2}\right)} \right] \right\}$$

After simplification, it becomes

$$E_{out}(t) = \frac{\sqrt{t_{ff}}}{2} E_0 \left\{ e^{i\xi_1\pi} + e^{i\xi_2\pi} + r \sum_{n=-\infty}^{\infty} \left[J_n(\xi\pi) e^{in(\omega t+\theta)} \left((-i)^n - i^{2n+1} \right) \right] \right\} \quad (4)$$

When n=0, the term corresponding to optical carrier is obtained

$$E_{\omega_c} = \frac{\sqrt{t_{ff}}}{2} E_0 \left[e^{i\xi_1\pi} + e^{i\xi_2\pi} + \sqrt{2} r J_0(\xi\pi) e^{-i\frac{\pi}{4}} \right]$$

When n=1, the upper RF fundamental component $E_{+\omega}$ is equivalent to 0. That means the upper RF sideband is eliminated.

When n=-1, the lower RF fundamental component of RF signal is symbolized as follows

$$E_{-\omega} = \sqrt{t_{ff}} E_0 r J_{-1}(\xi\pi) e^{-i\left(\omega t+\theta-\frac{1}{2}\pi\right)}$$

According to $J_{-m}(z) = (-1)^m J_m(z)$, $E_{-\omega} = -\sqrt{t_{ff}} E_0 r J_1(\xi\pi) e^{-i\left(\omega t+\theta-\frac{1}{2}\pi\right)}$

It is obvious that only the lower sideband exists after modulation and OSSB is achieved.

Furthermore, optical carrier-to-sideband ratio in power is also obtained

$$OCSR[dB] = \frac{2r^2 J_0(\xi\pi) + 2\cos(\xi_1 - \xi_2)\pi + 2rJ_0(\xi\pi)[\cos\xi_1\pi + \cos\xi_2\pi - \sin\xi_1\pi - \sin\xi_2\pi] + 2}{4r^2 J_1^2(\xi\pi)}$$

(5)

From (5), it is recognized that three parameters, ξ, ξ_1, and ξ_2, determine the value of OCSR. As defined above, they represent the amplitudes of RF signal, $1DC_{OP}$ and $2DC_{OP}$. In typical conventional OSSB system, OCSR only depends on ξ. Here, it is verified to

be feasible that our purpose of adjusting OCSR can be accomplished by sweeping ξ_1, and ξ_2. In Chapter 3, we will show how ξ, ξ_1, and ξ_2 exactly affect OCSR.

An EDFA is added after the parallel DE-MZMs in order to compensate the insertion loss of DE-MZM. The output optical signal after EDFA is

$$E_{EDFA}(t) = E_{out}(t)\sqrt{G_{EDFA}}$$

As the optical signal is detected by an ideal PD with responsivity $\Re$, the temporal expression of the current can be calculated from the envelope of the incident optical signal and expressed as follows

$$i_{pd}(t) = \frac{\Re E_{EDFA} E_{EDFA}^{*}}{2} = \frac{\Re t_{ff} G_{EDFA} E_0^2}{8}\left\{e^{i\xi_1\pi} + e^{i\xi_2\pi} + r\sum_{n=-\infty}^{\infty}\left[J_n(\xi\pi)e^{in(\omega t+\theta)}\left((-i)^n - i^{2n+1}\right)\right]\right\}\cdot$$
$$\left\{e^{-i\xi_1\pi} + e^{-i\xi_2\pi} + r\sum_{p=-\infty}^{\infty}\left[J_p(\xi\pi)e^{-ip(\omega t+\theta)}\left(i^p + i^{2p+1}\right)\right]\right\} \tag{6}$$

The optical carrier component beats with the first order component of RF signal, which makes foremost contribution to the final desired electrical signal. Finally, RF signal after PD can be represented as

$$I_\omega \approx \frac{\Re t_{ff} G_{EDFA} E_0^2}{2}\left|\begin{array}{l} -rJ_1(\xi\pi)\cos(\omega t+\theta+\xi_1\pi-\frac{\pi}{2}) - rJ_1(\xi\pi)\cos(\omega t+\theta+\xi_2\pi-\frac{\pi}{2}) + \\ \sqrt{2}r^2 J_0(\xi\pi)J_1(\xi\pi)\cos(\omega t+\theta+\frac{\pi}{4}) \end{array}\right| \tag{7}$$

In (7), there are three terms totally and the first two terms including ξ_1 and ξ_2 displays their influence on the final RF output power. From the discussion above, we make out ξ_1

and ξ_2 have a great impact on OCSR. Our purpose is to investigate how OCSR affects the final RF output power. In Chapter 3, the detailed investigation will be presented.

The optical spectra after our proposed modulator corresponding to (4) are shown in Fig. 2.5 (a) and the electrical spectra after photo detector corresponding to (6) are displayed in Fig. 2.5(b).

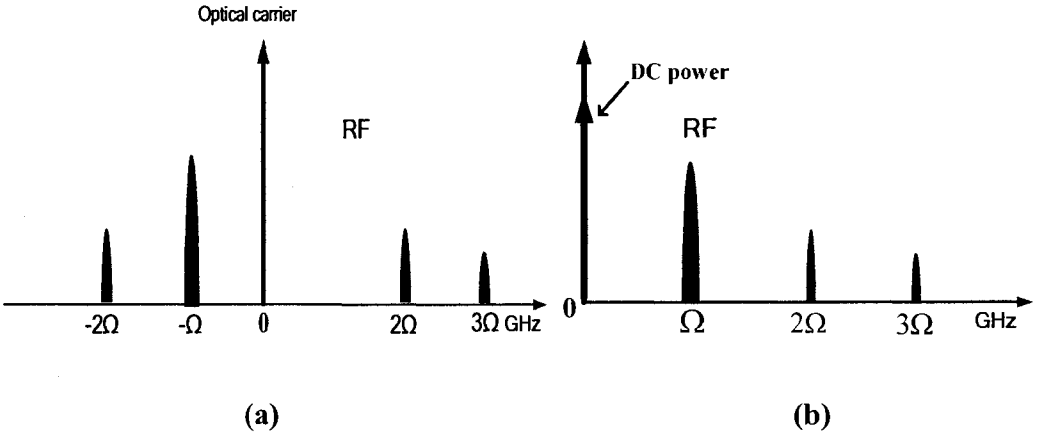

Fig. 2.5 (a) Optical and (b) electrical spectra of our proposed modulation

In (a), there exist optical carrier, single sideband sub-carrier and HDs at the frequencies of $\pm 2\omega$, 3ω and even higher order components appear after modulation. In (b), those components are converted into electrical domain after photo detector. When optical carrier beats with itself, a portion of DC power appears. When optical carrier beats with other RF components, fundamental, second order, third order and even higher order RF terms appear. This situation happens when one optical carrier carries only one RF sub-carrier. When two RF sub-carriers are used in our modulation, the situation changes greatly as new nonlinear components will appear. This will be discussed in the following part. HDs may degrade the

transmission performance in fiber-radio links very seriously. However, we can suppress or even filter out those terms easily by properly employing electrical filters after PD as the frequencies of those components are distant from that of the fundamental component. Therefore, the main noise source considered here is shot noise, thermal noise and ASE noise from EDFA. As OCSR varies, it has little influence on those noises. Enormous improvement of RF output power due to optimum OCSR can lead to immense improvement of SNR.

2.2.2 Proposed modulator driven by two RF signals

In this section, we investigate the situation in which one optical carrier carries two sub-carriers. Here, $1DC_{RF}$ and $2DC_{RF}$ are still set to 0 V and $\frac{V_\pi}{2}$ respectively. Comparing with Section 2.2.1, what we need to do is modify (1) and (2) as follows

$$V_1 = V_m\left[cos\left(\omega_1 t+\theta_1\right)+cos\left(\omega_2 t+\theta_2\right)\right] \tag{8}$$

$$V_2 = V_m\left[cos\left(\omega_1 t+\theta_1-\frac{\pi}{2}\right)+cos\left(\omega_2 t+\theta_2-\frac{\pi}{2}\right)\right] \tag{9}$$

ω_1 and ω_2 are the angular frequencies of the two input RF signals. θ_1 and θ_2 are the initial phases of the two input RF signals. With the same definition of ξ, ξ_1 and ξ_2, (3) becomes

$$E_{out}(t)=\frac{\sqrt{t_{ff}}}{2}E_0\left\{e^{i\xi_1\pi}+e^{i\xi_2\pi}+re^{-i\xi\pi\left[\cos\left(\omega_1 t+\theta_1\right)+\cos\left(\omega_2 t+\theta_2\right)\right]}+re^{-i\frac{\pi}{2}}e^{-i\xi\pi\left[\cos\left(\omega_1 t+\theta_1-\frac{\pi}{2}\right)+\cos\left(\omega_2 t+\theta_2-\frac{\pi}{2}\right)\right]}\right\} \tag{10}$$

We use Bessel function to expand it into

$$E_{out}(t)=\frac{\sqrt{t_{ff}}}{2}E_0\left\{\begin{array}{l} e^{i\xi_1\pi}+e^{i\xi_2\pi}+r\sum_{m=-\infty}^{\infty}\sum_{n=-\infty}^{\infty}i^{m+n}J_m(\xi\pi)J_n(\xi\pi)e^{i[m(\omega_1 t+\theta_1+\pi)+n(\omega_2 t+\theta_2+\pi)]} \\ +r\sum_{m=-\infty}^{\infty}\sum_{n=-\infty}^{\infty}i^{m+n}J_m(\xi\pi)J_n(\xi\pi)e^{i[m(\omega_1 t+\theta_1+\frac{\pi}{2})+n(\omega_2 t+\theta_2+\frac{\pi}{2})-\frac{\pi}{2}]} \end{array}\right\} \quad (11)$$

When both m and n are chosen at 0, the expression of optical carrier is obtained

$$E_{\omega_c}=\frac{\sqrt{t_{ff}}}{2}E_0\left[e^{i\xi_1\pi}+e^{i\xi_2\pi}+\sqrt{2}rJ_0{}^2(\xi\pi)e^{-i\frac{\pi}{4}}\right]$$

When m and n are fixed at +1 and n=0 respectively, the upper sideband fundamental component of RF1 signal $E_{+\omega_1}$ is equal to 0.

When m and n are fixed at -1 and 0 respectively, the lower sideband fundamental component of RF1 signal is as follows

$$E_{-\omega_1}=\sqrt{t_{ff}}E_0rJ_0(\xi\pi)J_{-1}(\xi\pi)e^{-i\left(\omega_1 t+\theta_1-\frac{1}{2}\pi\right)}$$

When m and n are fixed at 0 and +1 respectively, the upper sideband fundamental component of RF2 signal $E_{+\omega_2}$ is equal to 0.

When m and n are fixed at 0 and -1 respectively, the lower sideband fundamental component of RF2 signal is as follows

$$E_{-\omega_2}=\sqrt{t_{ff}}E_0rJ_0(\xi\pi)J_{-1}(\xi\pi)e^{-i\left(\omega_2 t+\theta_2-\frac{1}{2}\pi\right)}$$

Very evidently, the upper sideband fundamental components of both RF signals are eliminated and only lower ones are left. OSSB are achieved. The coefficients of $E_{-\omega_1}$ and $E_{-\omega_2}$ are equal to each other so it is reasonable to define OCSR of the two RF signals by employing one mathematical expression. It is also observed that only the coefficient of $J_0(\xi\pi)$ is coupled into both the optical carrier component and the RF fundamental components compared with the situation with one RF signal. The formula to

calculate OCSR here is completely identical to (5).

An EDFA is added after the parallel DE-MZMs in order to compensate the insertion loss of MZMs. The output light wave after EDFA is

$$E_{EDFA}(t) = E_{out}(t)\sqrt{G_{EDFA}}$$

As the optical signal is detected by an ideal PD with responsivity $\Re$, the temporal expression of the current can be calculated from the envelope of the incident optical signal and expressed as follows

$$i_{pd}(t) = \frac{\Re E_{EDFA} E_{EDFA}^{*}}{2} = \frac{\Re t_{ff} G_{EDFA} E_0^2}{8} \left\{ \begin{array}{l} e^{i\xi_1\pi} + e^{i\xi_2\pi} + \\ r\sum_{m=-\infty}^{\infty}\sum_{n=-\infty}^{\infty} i^{m+n} J_m(\xi\pi) J_n(\xi\pi) e^{i[m(\omega_1 t+\theta_1+\pi)+n(\omega_2 t+\theta_2+\pi)]} + \\ r\sum_{m=-\infty}^{\infty}\sum_{n=-\infty}^{\infty} i^{m+n} J_m(\xi\pi) J_n(\xi\pi) e^{i[m(\omega_1 t+\theta_1+\frac{\pi}{2})+n(\omega_2 t+\theta_2+\frac{\pi}{2})-\frac{\pi}{2}]} \end{array} \right\} \cdot$$

$$\left\{ \begin{array}{l} e^{-i\xi_1\pi} + e^{-i\xi_2\pi} + r\sum_{p=-\infty}^{\infty}\sum_{q=-\infty}^{\infty} (-i)^{p+q} J_p(\xi\pi) J_q(\xi\pi) e^{-i[p(\omega_1 t+\theta_1+\pi)+q(\omega_2 t+\theta_2+\pi)]} + \\ r\sum_{p=-\infty}^{\infty}\sum_{q=-\infty}^{\infty} (-i)^{p+q} J_p(\xi\pi) J_q(\xi\pi) e^{-i[p(\omega_1 t+\theta_1+\frac{\pi}{2})+q(\omega_2 t+\theta_2+\frac{\pi}{2})-\frac{\pi}{2}]} \end{array} \right\} \tag{13}$$

The optical carrier beats with the first order components of the two RF signals, which makes chief contribution to the final desired RF signals. Finally, RF1 and RF2 signal after PD can be represented as

$$I_{\omega_1} \approx \frac{\Re t_{ff} G_{EDFA} E_0^2}{2} \left[\begin{array}{l} -rJ_0(\xi\pi)J_1(\xi\pi)\cos(\omega_1 t+\theta_1+\xi_1\pi-\frac{\pi}{2}) \\ -rJ_0(\xi\pi)J_1(\xi\pi)\cos(\omega_1 t+\theta_1+\xi_2\pi-\frac{\pi}{2}) \\ +\sqrt{2}r^2 J_0^{\,3}(\xi\pi)J_1(\xi\pi)\cos(\omega_1 t+\theta_1+\frac{\pi}{4}) \end{array} \right] \tag{14}$$

$$I_{\omega_2} \approx \frac{\Re t_{ff} G_{EDFA} E_0^2}{2} \begin{bmatrix} -rJ_0(\xi\pi)J_1(\xi\pi)\cos(\omega_2 t + \theta_2 + \xi_1\pi - \frac{\pi}{2}) \\ -rJ_0(\xi\pi)J_1(\xi\pi)\cos(\omega_2 t + \theta_2 + \xi_2\pi - \frac{\pi}{2}) \\ +\sqrt{2}r^2 J_0^3(\xi\pi)J_1(\xi\pi)\cos(\omega_2 t + \theta_2 + \frac{\pi}{4}) \end{bmatrix} \quad (15)$$

Comparing (14) with (15), the expressions are almost the same except the parameters of frequencies and initial phases. Both (14) and (15) consist of three terms which indicate the influence of ξ, ξ_1 and ξ_2.

The optical spectra after EDFA corresponding to (11) and the electrical spectra after PD corresponding to (13) are shown in Fig. 2.6.

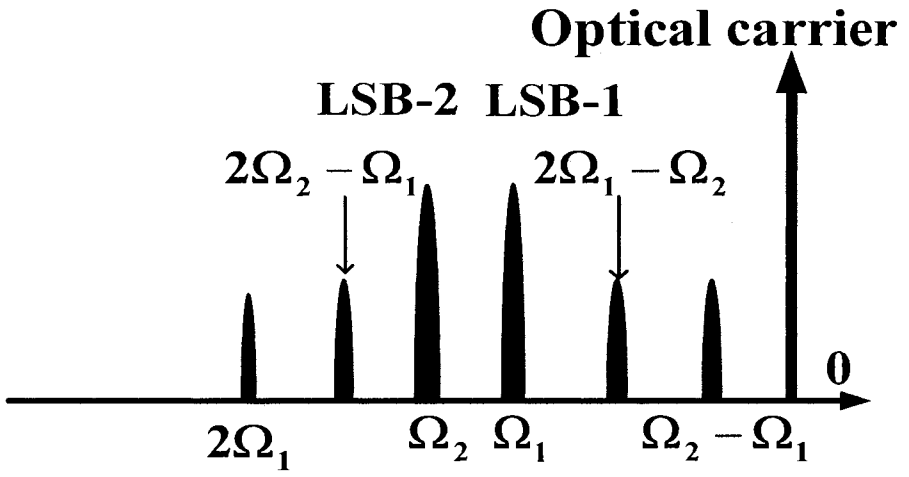

(a)

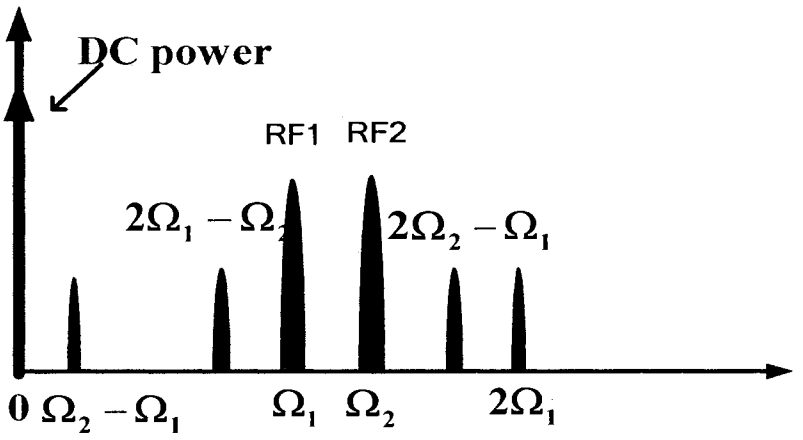

(b)

Fig. 2.6 (a) Optical spectra after EDFA (b) electrical spectra after photodetector

In Fig. 2.6, it is displayed that not only HD terms of ω_1 and ω_2 but also IMD terms between ω_1 and ω_2 happen. The IMD terms like $\pm(\omega_1-\omega_2), \pm(2\omega_1-\omega_2), \pm(2\omega_2-\omega_1)$ and higher order terms may degrade the transmission performance in fiber-radio links more severely than harmonic distortion. Especially third order inter-modulations $\pm(2\omega_1-\omega_2), \pm(2\omega_2-\omega_1)$ may have most severe negative effect on SNR of the output RF signals because they are normally close to the fundamental components and hard to be suppressed or filtered out. It is necessary to figure out how OCSR influences IM3. Furthermore, we don't incorporate standard single mode fibers in our analytical model to avoid chromatic dispersion from fibers. In that case, the relationship between OCSR and IM3 can be displayed more directly and clearly. The exact expressions of IM3 components are shown here

$$I_{2\omega_1-\omega_2}=\frac{\Re t_{ff}G_{EDFA}E_0^2}{2}\begin{bmatrix} rJ_1(\xi\pi)J_2(\xi\pi)\cos(2\omega_1 t-\omega_2 t+2\theta_1-\theta_2+\xi_1\pi-\frac{\pi}{2}) \\ +rJ_1(\xi\pi)J_2(\xi\pi)\cos(2\omega_1 t-\omega_2 t+2\theta_1-\theta_2+\xi_2\pi-\frac{\pi}{2}) \\ -\sqrt{2}r^2J_0{}^2(\xi\pi)J_1(\xi\pi)J_2(\xi\pi)\cos(2\omega_1 t-\omega_2 t+2\theta_1-\theta_2-\frac{\pi}{4}) \end{bmatrix} \quad (16)$$

$$I_{2\omega_2-\omega_1}=\frac{\Re t_{ff}G_{EDFA}E_0^2}{2}\begin{bmatrix} rJ_1(\xi\pi)J_2(\xi\pi)\cos(2\omega_2 t-\omega_1 t+2\theta_2-\theta_1+\xi_1\pi-\frac{\pi}{2}) \\ +rJ_1(\xi\pi)J_2(\xi\pi)\cos(2\omega_2 t-\omega_1 t+2\theta_2-\theta_1+\xi_2\pi-\frac{\pi}{2}) \\ -\sqrt{2}r^2J_0{}^2(\xi\pi)J_1(\xi\pi)J_2(\xi\pi)\cos(2\omega_2 t-\omega_1 t+2\theta_2-\theta_1-\frac{\pi}{4}) \end{bmatrix} \quad (17)$$

In both (16) and (17), the first two terms include ξ_1 and ξ_2, which represent $1DC_{OP}$ and $2DC_{OP}$.

Chapter 3 Simulation and comparison with theoretical analysis

In this chapter, our proposed modulation technique is verified by computer simulations. All the simulations are based on the platform of VPI TransmissionMaker 7.0, a commercial software package.

The parameters of CW laser are configured as in Table 1. Emission Frequency indicates the central emission frequency of laser and determines the wavelength of emitted light wave. Average Power specifies the power of output light wave. Line Width characterizes the width of the frequency interval of total emission area. Initial Phase gives the initial phase of oscillation to generate light wave.

Table 1 CW laser parameters

Emission frequency (Hz)	193.1×10^{12}
Average power (w)	1.0×10^{-3}
Line width (Hz)	10×10^{6}
Initial phase (°)	0

The parameters of parallel DE-MZMs are configured as in Table 2. $V_{\pi DC}$ specifies DC voltage required (at both split electrodes) for π phase difference. $V_{\pi RF}$ indicates RF voltage required (at both split electrodes) for π phase difference. Insertion Loss gives the insertion loss of DE-MZM. Extinction Ratio characterizes the power division ratio of upper path to lower path in a single DE-MZM.

Table 2 DE-MZM parameters

$V_{\pi DC}$ (V)	5
$V_{\pi RF}$ (V)	5
Insertion loss (dB)	6
Extinction ratio (dB)	15

The EDFA used in the simulation is assumed noise-free and the fixed output power mode is chosen as its output mode. In Section 3.1.1, optical fiber with the length of 25 km is employed to investigate how chromatic dispersion influences the performance of our system. In order to compensate the attenuation loss caused by optical fiber, the output power of EDFA is fixed at 0 dBm. For the rest of the simulation, we choose the ideal connection instead of single mode optic fiber between EDFA and PD in order to clearly evaluate the improvement resulted from our modulation technique. In addition, the optical power of incident optical signal on PD can never be larger than 0 dB, which is the saturation value of PD. Therefore, the output power is fixed at -5 dBm when one RF signal is applied, while the output power is -1 dBm with the input of two RF signals.

The PD parameters are configured as in Table 3. Responsivity specifies the current generated per unit optical power. Here, we employ an ideal PD so its responsivity is 1 A/W. Dark current characterizes the current generated by the photodiode when it is not illuminated. The ideal PD is assumed in this table. Thermal Noise represents the spectral density of thermal noise. Shot Noise "off" indicates the noise mechanism in our

simulations is not considered.

Table 3 PD parameters

Responsivity (A/W)	1
Dark current (A)	0.0
Thermal noise ($A/\sqrt{Hz}$)	10.0×10^{-12}
Shot noise	Off

3.1 Proposed modulator driven by one RF signal

3.1.1 Optical single sideband modulation with adjustable optical carrier-to-sideband ratio

The greatest attraction of our modulation technique is that not only the value of OCSR can be adjusted, but also OSSB optical signal is obtained. In the RoF systems where IM-DD is used, the value of OCSR represents the modulation efficiency. When OCSR is large, it signifies considerably low modulation efficiency; when OCSR is small, it means high modulation efficiency. Basically, modulation index (MI) determines the value of OCSR. Large MI is able to suppress OCSR and lead to high modulation efficiency. Reversely, when RF signal of small MI is applied to modulate light wave, OCSR is considerably large and the modulation efficiency is low. However, the nonlinear distortions *i.e.* HDs and IMDs are little in small-MI cases. If we can improve modulation efficiency when MI is small, it will significantly improve system performance. In this

thesis, the goal of our modulation technique is to improve modulation efficiency and optimize OCSR by sweeping DC_{OP}. In this section, we first show how DC_{OP} greatly affects OCSR, and in Section 3.1.2, we will present the detailed description regarding how DC_{OP} pair and RF pair influence OCSR. Fig. 3.1 illustrates a set of four optical spectrums after EDFA under different DC_{OP} in MI=0.05 case.

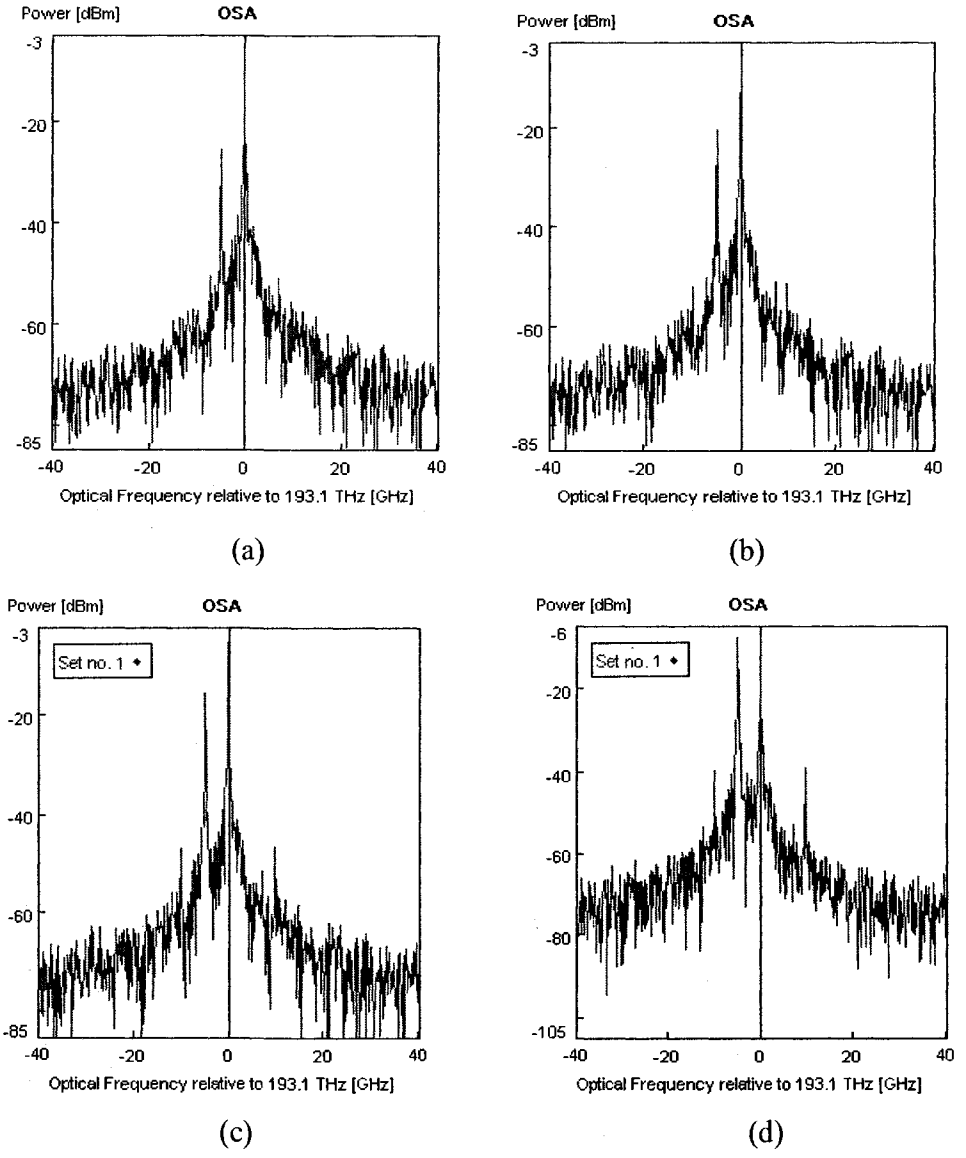

Fig. 3.1 Optical spectra after EDFA under different $1DC_{OP}$ (a) $1DC_{OP}$=0 V; (b) $1DC_{OP}$=1.0 V; (c) $1DC_{OP}$=1.4 V; (d) $1DC_{OP}$=2.1 V.

In Fig. 3.1, it is displayed that the upper sideband RF components are eliminated and only the lower sideband RF components exist in all four situations. In fact, DC_{RF} determines whether upper sideband or lower sideband will be eliminated. Here, $1DC_{RF}$ and $2DC_{RF}$ are set to 0 V and $\frac{V_\pi}{2}$ respectively and it leads to a lower single sideband modulation. If we exchange their values, lower sideband RF components will be eliminated and only upper sideband RF components will be preserved. In Fig. 3.1 (a), $1DC_{OP}$ and $2DC_{OP}$ are set to 0 V, 5.3 V respectively and OCSR is equal to 20 dB. To some extent, this situation is similar to the typical optical single sideband modulation, and the modulation efficiency is extremely low. However, the second order harmonics which makes main contribution to the nonlinear distortion can be negligible. In Fig. 3.1 (b), $2DC_{OP}$ keeps the same and $1DC_{OP}$ is shifted to 1.0 V and it results in suppressing OCSR to 15 dB. The second order harmonics are still awfully tiny. In Fig. 3.1 (c), $1DC_{OP}$ is increased to 1.4 V while $2DC_{OP}$ keeps fixed, and OCSR decreases to 10 dB. In addition, the second order harmonics become slightly noticeable. In Fig. 3.1 (d), $1DC_{OP}$ is fixed at 2.1 V and OCSR arrives at 0 dB. The second order harmonics in Fig. 3.1 (d) are much more observable than those in Fig. 3.1 (c). As a matter of fact, 0 dB is the optimum value for OCSR when only one RF signal is applied, because decreasing the value of OCSR will increase the RF output power, thus maximum RF output power will happen when OCSR is equal to 0 dB. In Section 3.1.2, we will introduce more details about how we maximize the performance of system by optimizing OCSR.

The preference of OSSB to ODSB is because that it can overcome the chromatic

dispersion. Chromatic dispersion is caused by the different wavelength-dependent propagation time of different spectral components. In ODSB RoF systems, chromatic dispersion can cause time lag between carrier and sidebands. When both upper sideband and lower sideband beat with optical carrier in PD, the propagation time lag between the two sidebands represents their phase difference. If the phase difference is large enough, it can cause suppression of the transmitted signals at certain transmission length. Especially if the frequency of the RF signal is remarkably high, chromatic dispersion can greatly degrade the transmission performance. The transmission distances of high frequency microwave signals are also severely limited by chromatic dispersion. For instance, the transmission distance of a 60 GHz millimeter wave is limited to less than 2 km on standard single mode fiber at the wavelength of 1550 nm.

To show the chromatic dispersion's impact on our system, the distribution of RF signals with different frequencies is simulated. The simulation is carried out at the wavelength of 1550 nm with a dispersion parameter of 16 $ps/nm \cdot km$, which is equal to that of standard SMF. The fiber length is 25 km. The frequency of RF signal varies from 1 GHz to 25 GHz. $1DC_{OP}$, $2DC_{OP}$, $1DC_{RF}$ and $2DC_{RF}$ are set to 2.1 V, 5.3 V, 0 V and 2.5 V respectively. Fig. 3.2 shows the plot of the RF output power loss versus the frequency of input RF signal. The simulation result of the typical ODSB IM-DD system is included for the purpose of comparison.

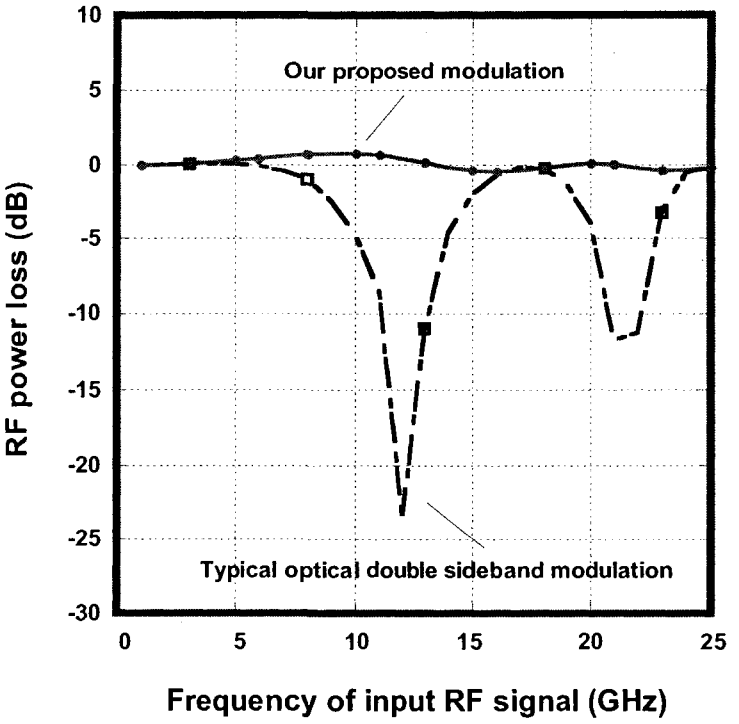

Fig. 3.2 RF power loss in our proposed modulation and ODSB

Fig. 3.2 shows the amplitude suppression in the typical ODSB IM-DD system caused by chromatic dispersion. Two nulls are encountered respectively at the frequencies of 12 GHz and 22 GHz. For our modulation technique, no null is present regardless radio frequencies are utilized. The fluctuation of the RF power loss is within 0.5 dB. Therefore, we make a conclusion that our modulation technique is robust against chromatic dispersion.

3.1.2 Impact of $1DC_{OP}$ and $2DC_{OP}$ on OCSR

As we referred in Section 1.3, weakly modulated optical signals represent large OCSR, and the huge optical power difference between the mm-wave RF sideband and optical carrier indicates low modulation efficiency. Although nonlinear distortion is almost

negligible in small MI cases, the application of small MI is worthless in RoF system because the optical carrier carries most of the power without any information and it is a waste of system resource. The goal of our modulation technique is to improve the modulation efficiency by adjusting the inputs of DC_{OP} pair and RF pair. In Section 3.1.1, we showed how $1DC_{OP}$ and $2DC_{OP}$ influence OCSR and it is proved that OCSR is adjustable by using our proposed modulation technique. Furthermore, we show how $1DC_{OP}$, $2DC_{OP}$ and MI affect OCSR by plotting the corresponding curves. We set the RF frequency f=5GHz and choose the amplitudes of RF signal V_m at 0.25, 0.5, 1, 2.5 respectively. If V_m is expressed by MI, the values are 0.05, 0.1, 0.2 and 0.5. MI = 0.05 and 0.1 represent the extra small MIs; MI = 0.2 and 0.5 represent the small and medium MI respectively. For the adjustment of OCSR, the effect of sweeping $1DC_{OP}$ while keeping $2DC_{OP}$ fixed is equivalent to that of sweeping $2DC_{OP}$ while keeping $1DC_{OP}$ fixed. In the thesis, we sweep $1DC_{OP}$ and fix the normalized value of $2DC_{OP}$, ξ_2, at 1.06 for both extra small and small MIs, while ξ_2 is placed to 0 for medium MI. In the following figures, the results of theoretical analysis are also illustrated and compared with the simulation results.

Case1 (MI=0.05): we sweep $1DC_{OP}$ from 0 V to 5V and the results are plotted in Fig. 3.3.

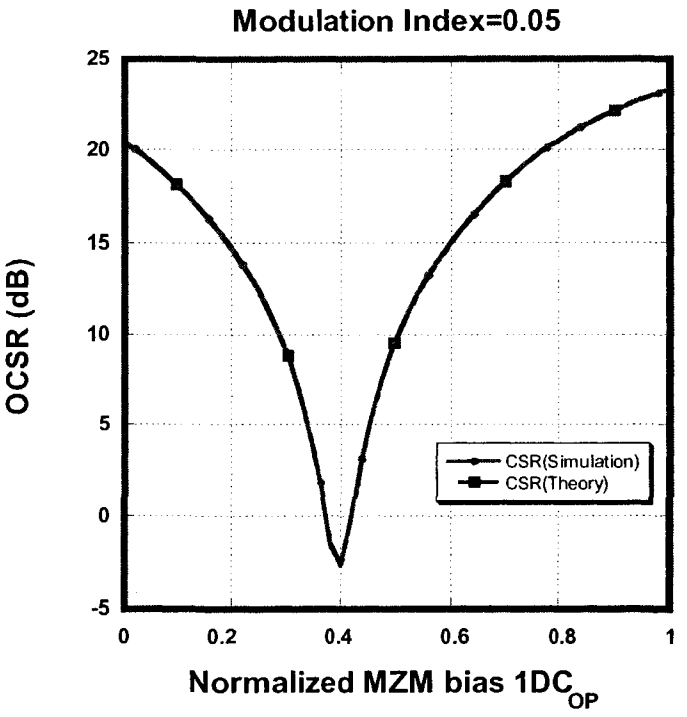

Fig. 3.3 Impact of ξ_1 (normalized MZM bias $1DC_{OP}$) on OCSR when MI=0.05

In Fig. 3.3, OCSR decreases smoothly from 20.5 dB to 15 dB as we increase the value of ξ_1 from 0 to 0.2. While the value of ξ_1 is increased from 0.2 to 0.4, OCSR keeps decreasing until -2.7 dB and the slope of OCSR becomes sharper. After that, OCSR begins to increase swiftly and return to positive at the point of ξ_1=0.42. The curve of OCSR is symmetrical by the axis of ξ_1=0.4. In the interval between ξ_1=0.36 to ξ_1=0.42, the optical carrier is greatly suppressed that its power level is smaller than that of the sideband, which makes the value of OCSR be negative. Finally, the OCSR is decreased by 25.8 dB and the modulation efficiency is extremely improved.

Case 2 (MI=0.1): we sweep $1DC_{OP}$ from 0 V to 5 V and the results are plotted in Fig. 3.4.

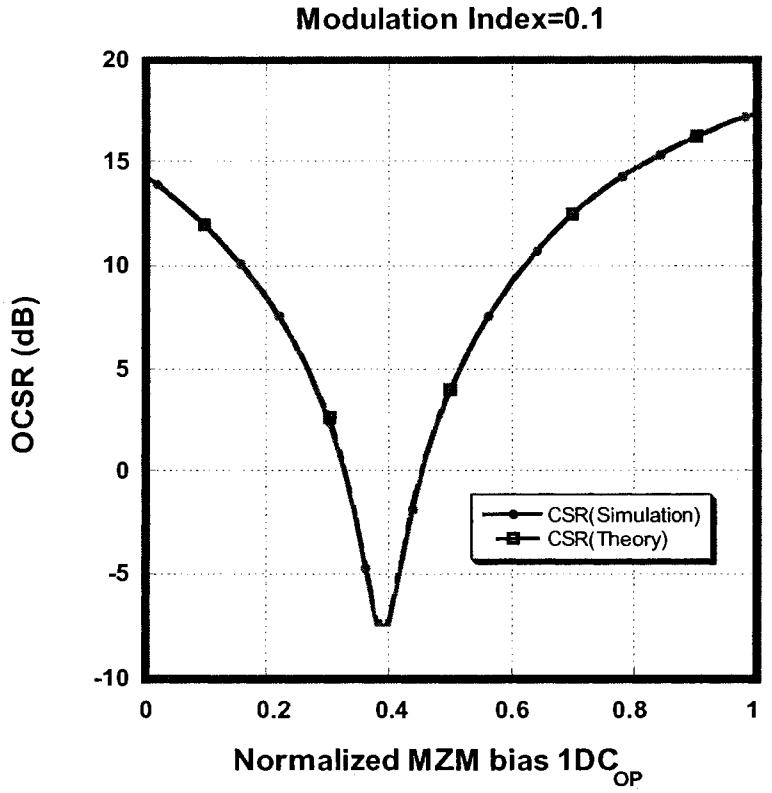

Fig. 3.4 Impact of ξ_1 (normalized MZM bias $1DC_{OP}$) on OCSR when MI=0.1

In Fig. 3.4, OCSR decreases smoothly from 14.3 dB to 12 dB as we increase the value of ξ_1 from 0 to 0.2. While the value of ξ_1 is increased from 0.2 to 0.4, OCSR keeps decreasing until -7.4 dB and the slope of OCSR becomes sharper. After that, OCSR begins to increase swiftly and return to positive at the point of ξ_1=0.46. The curve of OCSR is symmetrical by the axis of ξ_1=0.39. In the interval between ξ_1=0.32 to ξ_1=0.46, the optical carrier is greatly suppressed that its power level is 7.4 dB smaller than that of the sideband, which makes the value of OCSR be negative. Finally, the OCSR is decreased by 24.9 dB and the modulation efficiency is extremely improved.

Case 3 (MI=0.2): we sweep$1DC_{OP}$ from 0 V to 5 V and the results are plotted in Fig. 3.5.

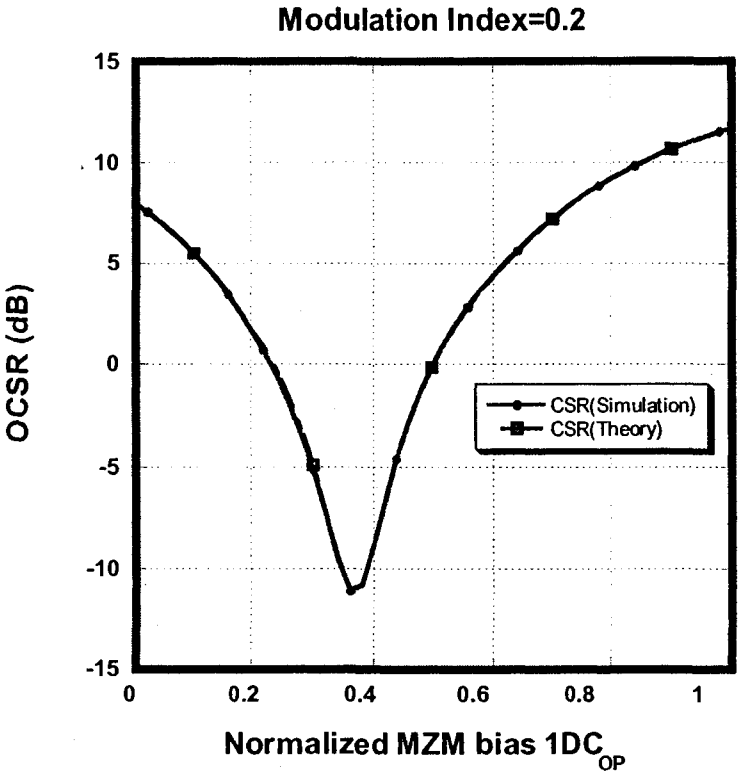

Fig. 3.5 Impact of ξ_1 (normalized MZM bias $1DC_{OP}$) on OCSR when MI=0.2

In Fig. 3.5, OCSR decreases smoothly from 8.0 dB to 5.5 dB as we increase the value of ξ_1 from 0 to 0.1. While the value of ξ_1 is increased from 0.2 to 0.37, OCSR keeps decreasing until -11 dB and the slope of OCSR becomes sharper. After that, OCSR begins to increase swiftly and return to positive at the point of ξ_1=0.5. The curve of OCSR is symmetrical by the axis of ξ_1=0.37. In the interval between ξ_1=0.22 to ξ_1=0.5, the optical carrier is greatly suppressed that its power level is 11 dB smaller than that of the sideband, which makes the value of OCSR be negative. Finally, the OCSR is decreased by 22.7 dB and the modulation efficiency is extremely improved.

Case 4 (MI=0.5): we sweep $1DC_{OP}$ from 0 V to 5 V and the results are plotted in Fig. 3.6.

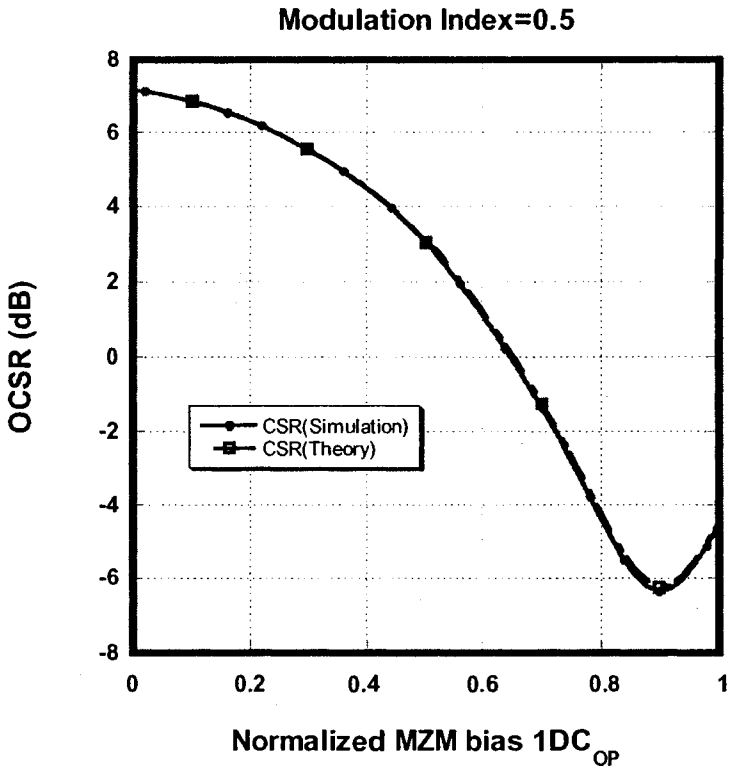

Fig. 3.6 Impact of ξ_1 (normalized MZM bias $1DC_{OP}$) on OCSR when MI=0.5

In Fig. 3.6, OCSR decreases lightly from 7.2 dB to 4.5 dB as we increase the value of ξ_1 from 0 to 0.4. Then the curve decreases very quickly until -6.4 dB. After that, OCSR begins to increase swiftly. The optical carrier is greatly suppressed that its power level is 6.4 dB smaller than that of the sideband, which makes the value of OCSR be negative. Finally, the OCSR is decreased by 13.5 dB and the modulation efficiency is extremely improved.

In Fig. 3.3 ~ Fig. 3.6, the theoretical results agree very well with the simulation results. We have to mention that there are some negligible discrepancies due to the errors of numerical calculation.

According to the four figures above, we make a conclusion that OCSR can be handily

adjusted within a large range by setting $1DC_{OP}$ and $2DC_{OP}$ properly. The upper boundary of the range may reach over 20 dB and the lower boundary may arrive at -11 dB. When both $1DC_{OP}$ and $2DC_{OP}$ are set to 0, the effect of our modulation technique is equal to that of typical OSSB. Therefore, we can observe the modulation efficiency of typical OSSB at the point of $\xi_1=0$ from Fig. 3.3 ~ Fig. 3.5. For detail, the values of OCSR corresponding to MI=0.05, 0.1, 0.2 are 20.4 dB, 14.3 dB, 8 dB respectively. In Section 1.3, we mentioned that 0 dB is the optimum value for OCSR to maximize the performance of one RF sub-carrier system. We define the effective improvement of OCSR as the difference between the initial OCSR (the OCSR corresponding to typical OSSB) and the optimum OCSR, thus the improvements under our definition are 20.4 dB, 14.3 dB and 8 dB corresponding to MI=0.05, 0.1 and 0.2. It can be concluded that our modulation technique is more effective and efficient to improve OCSR in small MI cases than in large MI cases.

Referring to Fig. 2.1, the phases of the optical carriers along Path1 and Path3 are shifted by a constant when $1DC_{OP}$ and $2DC_{OP}$ bias are fixed, even though the values of MIs are different. As introduced in Chapter 1, our modulation technique uses phase shifted optical carriers along Path1 and Path3, E_1+E_3, to interfere with RF modulated optical carriers along Path2 and Path4, E_2+E_4. In case of E_1+E_3 and E_2+E_4 have identical phase, the constructive interference will happen; otherwise, the destructive interference between two terms will happen. If E_1+E_3 have a π-phase difference from E_2+E_4, the final optical carrier will be suppressed most *i.e.* the most negative values of OCSR in Fig. 3.3

~ Fig. 3.6. The phase shift of optical carrier E_1+E_3 depends merely on $1DC_{OP}$ and $2DC_{OP}$, thus the improvements of OCSR when MI=0.05, 0.1 and 0.2 should almost be the same due to the identical value of $2DC_{OP}$ and sweeping range of $1DC_{OP}$. After OCSR decreases to the minimum, it starts to increase along the symmetrical track as the decreasing track. We can claim that all the curves are symmetrical by an approximately identical axis (ξ_1=0.4, ξ_1=0.39 and ξ_1=0.37). These are due to the same phase shift range caused by the identical $2DC_{OP}$ and the same sweeping range of $1DC_{OP}$. The slight differences of both OCSR improvement range and axis are caused by difference initial phase of the RF modulated optical carriers along Path2 and Path4. Moreover, we can also predict that all the curves are periodic, because of the characteristic of DE-MZM. In our DE-MZM, the voltage inducing π-phase shift is 5 V, which means the phase of optical carrier experience π shift when optical carrier goes through the path driven by 5 V. So when 10 V is employed, no change will happen to its phase.

3.1.3 Impact of OCSR on RF output power and SNR

According to [21], OCSR places enormous influence on the transmission performance in the fiber-radio links. Smaller OCSR indicates higher modulation efficiency and 0 dB is the optimum value for OCSR. In this section, we use two parameters, RF output power and SNR, to measure and quantify the improvement caused by our modulation technique. As mentioned in Section 1.2.4, only HDs exist when one RF signal is applied to modulate optical carrier. In Fig. 2.4, we can find HD terms are so far away from fundamental RF

sideband that it can be easily filtered out by electrical filters after PD. Therefore, in this case, only shot noise and thermal noise are considered as the noise sources. Our theoretical analysis verifies that OCSR has little influence on these noise sources.

Case 1 (MI=0.05): we measure the RF output power and SNR with different OCSR and the results are shown in Fig. 3.7 and Fig. 3.8.

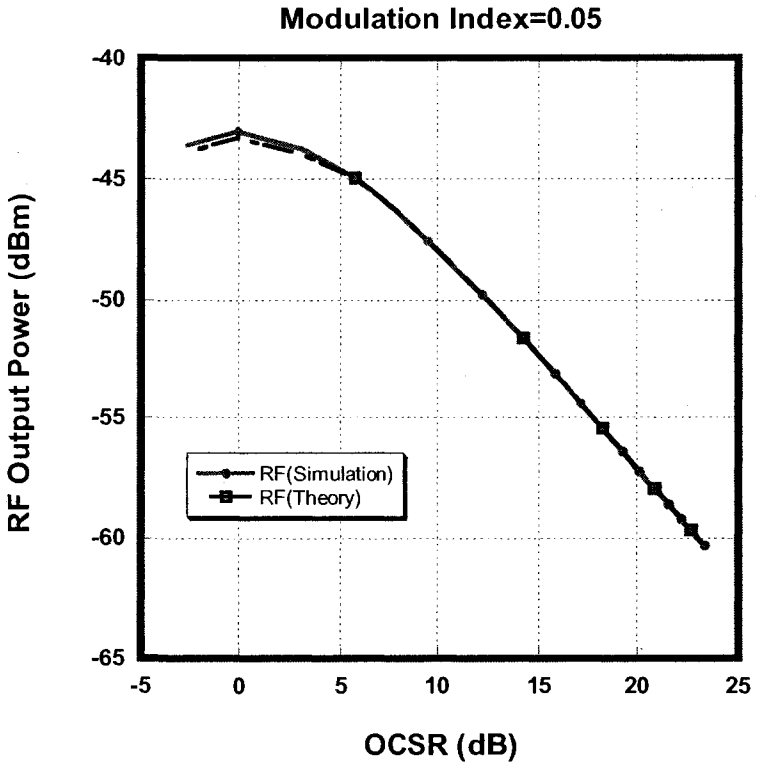

Fig. 3.7 Impact of OCSR on RF output power when MI=0.05

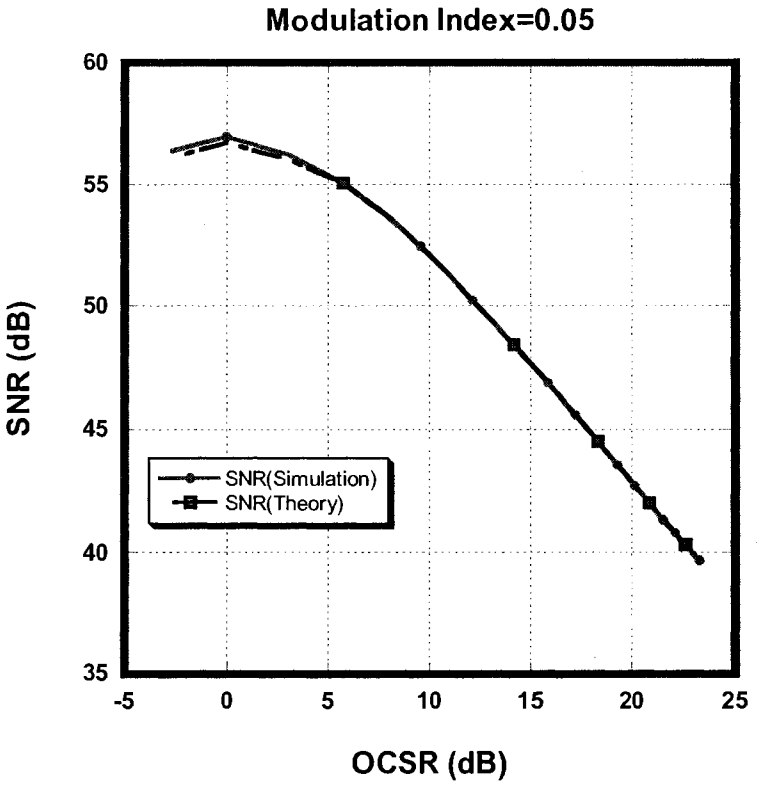

Fig. 3.8 Impact of OCSR on SNR when MI=0.05

As can be seen in Fig. 3.7 and Fig. 3.8, the curves have the relatively same shape, which proves that the noise power changes negligibly and can be considered as a constant. Both RF output power and SNR increase evidently when OCSR decreases from the initial point of OCSR=23.2dB. When OCSR measures up to 0 dB, both the RF output power and SNR reach the peak value. After that, they start to decrease. It is well-shown in both figures that the optimum value of OCSR is 0 dB so as to maximize the RF output power and SNR. The total improvements of them are 17.1 dB and 16.9 dB respectively.

Case 2 (MI=0.1): we measure the RF output powers and SNR under different OCSR and the results are plotted in Fig. 3.9 and Fig. 3.10.

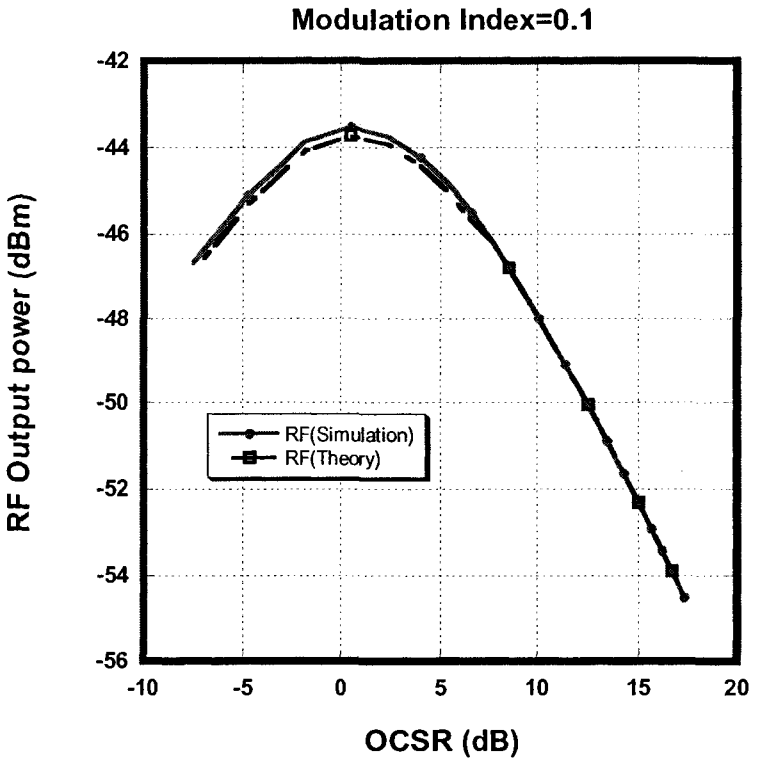

Fig. 3.9 Impact of OCSR on RF output power when MI=0.1

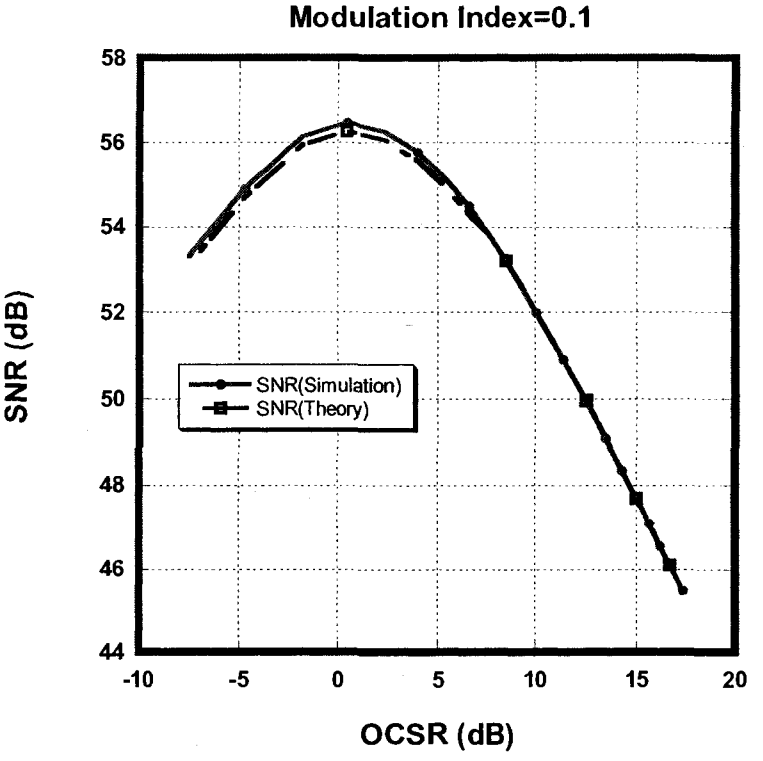

Fig. 3.10 Impact of OCSR on SNR when MI=0.1

As can be seen in Fig. 3.9 and Fig. 3.10, the curves have the same shape, which proves that the noise power changes negligibly and can be considered as a constant. Both RF output power and SNR increase evidently when OCSR decreases from the initial point of OCSR=17.3 dB. When OCSR measures up to 0 dB, both the RF output power and SNR reach the peak value. After that, they start to decrease. It is well-shown in both figures that the optimum value of OCSR is 0 dB so as to maximize the RF output power and SNR. The total improvements of them are 11.1 dB and 10.9 dB respectively.

Case 3 (MI=0.2): we measure the RF output powers and SNR under different OCSR and the results are plotted in Fig. 3.11 and Fig. 3.12.

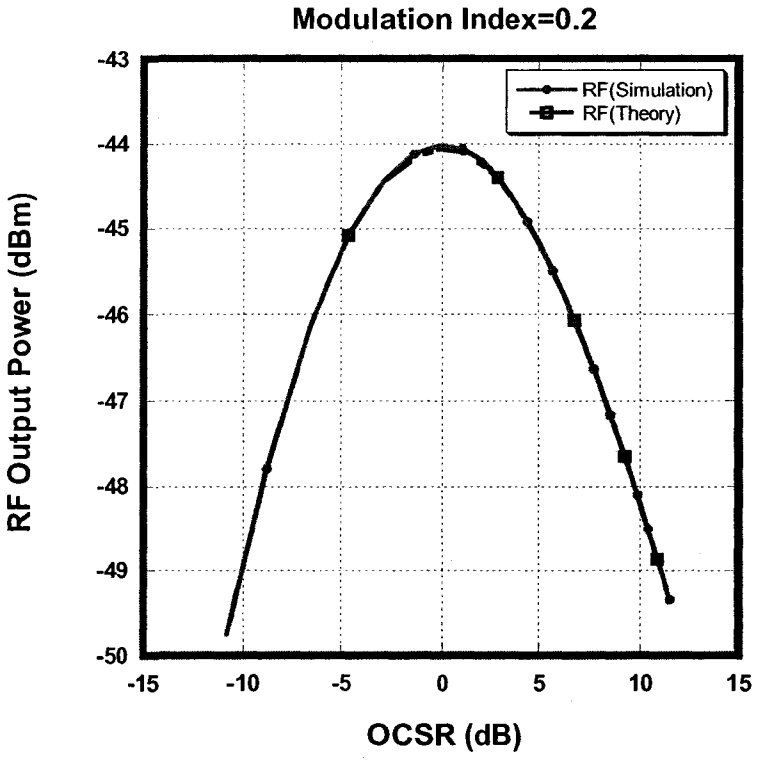

Fig. 3.11 Impact of OCSR on RF output power when MI=0.2

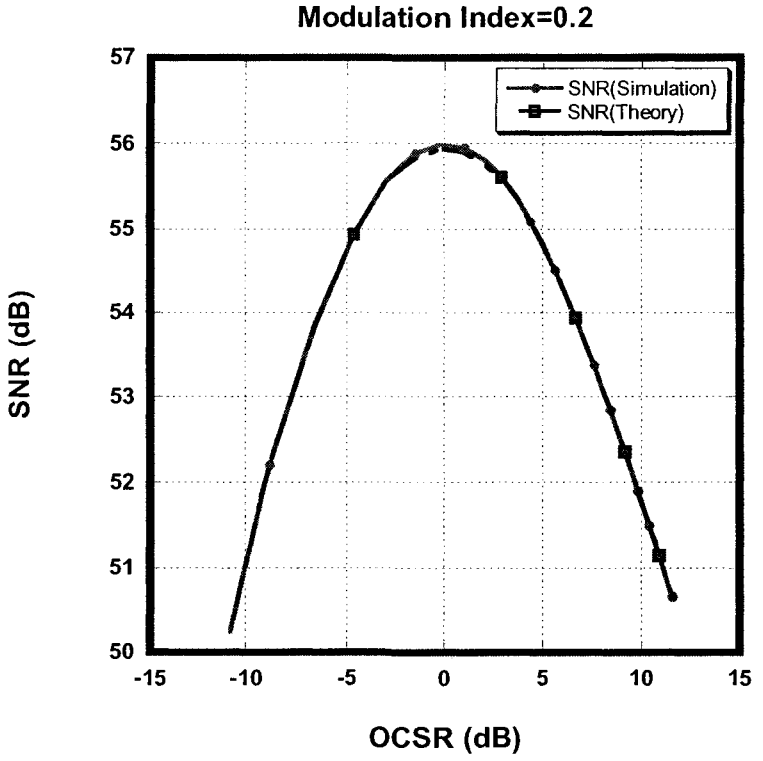

Fig. 3.12 Impact of OCSR on SNR when MI=0.2

As can be seen in Fig. 3.11 and Fig. 3.12, the curves have the relatively same shape, which proves that the noise power changes negligibly and can be considered as a constant. Both RF output power and SNR increase evidently when OCSR decreases from the initial point of OCSR=11.7 dB. When OCSR measures up to 0 dB, both RF output power and SNR reach the peak value. After that, they start to decrease. It is well-shown in both figures that the optimum value of OCSR is 0 dB so as to maximize the RF output power and SNR. The total improvements of them are 5.2 dB and 5.0 dB respectively.

Case 4 (MI=0.5): we measure the RF output powers and SNR under different OCSR and the results are plotted in Fig. 3.13 and Fig. 3.14.

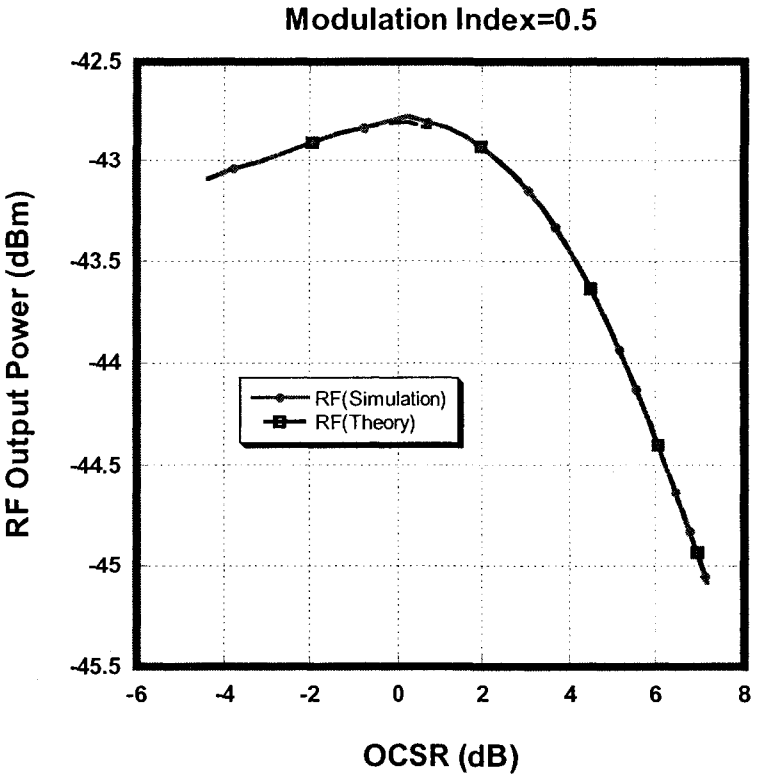

Fig. 3.13 Impact of OCSR on RF output power when MI=0.5

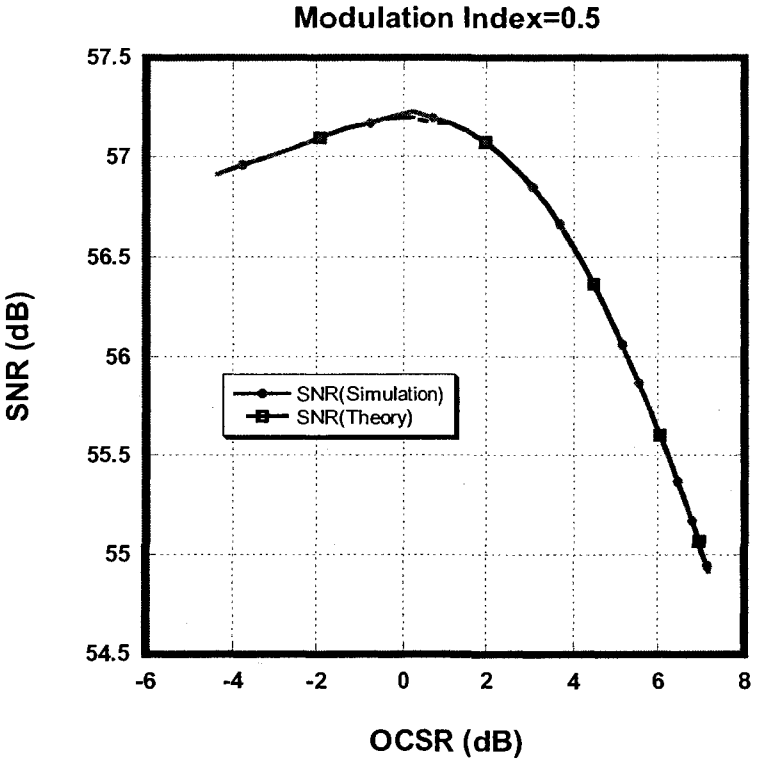

Fig. 3.14 Impact of OCSR on SNR when MI=0.5

As can be seen in Fig. 3.13 and Fig. 3.14, the curves have the relatively same shape, which proves that the noise power changes negligibly and can be considered as a constant. Both RF output power and SNR increase evidently when OCSR decreases from the initial point of OCSR=7 dB. When OCSR measures up to 0 dB, both RF output power and SNR reach the peak value. After that, they start to decrease. It is well-shown in both figures that the optimum value of OCSR is 0 dB so as to maximize the RF output power and SNR. The total improvements of them are 2.3 dB and 2.1 dB respectively.

All the curves from numerical analysis agree very well with those from analytical analysis, except of very little discrepancy due to the numerical calculation errors, the rest portions of results exactly match up with each other.

The figures above in this section indicate that when the absolute value of OCSR decreases, both RF output power and SNR increase, which achieve the maximum values at OCSR=0 dB. In the case of MI=0.05, the optimum OCSR happens at the point of ξ_1=0.42, ξ_2=1.06, while the RF output power and SNR achieve the improvements of 17.1 dB and 16.9 dB respectively. In the case of MI=0.1, the optimum OCSR happens at the point of ξ_1=0.46, ξ_2=1.06 while the RF output power and SNR achieve the improvements of 11.1 dB and 10.9dB respectively. In the case of MI=0.2, the optimum OCSR happens at the point of ξ_1=0.52, ξ_2=1.06 while RF output power and SNR gain 5.2 dB and 5.0 dB improvement respectively. In MI=0.5 case, the optimum OCSR happens at the point of ξ_1=0.64, ξ_2=0 while the RF output power and SNR achieve the improvements of 2.3 dB and 2.1 dB respectively. Based on those four cases, we make a conclusion that our

proposed modulation technique is much more effective in small MI cases than in large MI cases.

Why the improvement in small-MI cases is much greater than those in large-MI cases can be explained from two aspects. First, the effective adjustable range of OCSR is different. In small-MI cases, OCSR can be improved a lot because optical signal is very weakly modulated. If the effective OCSR range is large, we can make great improvement of RF output power and SNR. Second, HDs are different. Small MI leads to negligible HDs compared with fundamental RF component and optical carrier. When the modulated optical signal with suppressed optical carrier is amplified by EDFA, the fundamental RF component and optical carrier gain almost all the pump power from EDFA and nearly no power is consumed by HD terms. However, as MI increases, the HDs become larger and consume certain portion of pump power while amplified by EDFA, which wastes lots of energy and makes the modulation technique less efficient.

The situation that an optimum OCSR exists is due to interplay the optical power between optical carrier and sideband and the RF output power and SNR mainly depends on the square root of the product of optical carrier and sideband. When the output power of EDFA is fixed at -5dBm, the sum of optical carrier and sideband is almost a constant, and their product increases when the power value of optical carrier and sideband get close to each other. When their power value is identical, 0 dB OCSR is obtained, and their product reaches the peak point. RF output power and SNR are maximized by optimizing OCSR.

3.1.4 Phase sensitivity of proposed modulation technique

Our proposed modulation technique consists of two DE-MZMs which locates upper and lower branch respectively. In both theoretical analysis and simulation, we assume that Branch1 and Branch2 have identical initial phase. However, it is not applicable in practical uses. The different initial phase along the two branches may cause phase imbalance of the two parallel DE-MZMs. Thus it is highly necessary to investigate whether modulation efficiency is sensitive to the phase imbalance of the two parallel DE-MZMs. In the simulation, we insert a phase modulator after DE-MZM1. The phase modulator is driven by a DC source and the value is set to 0.06V. The initial phases of the phase modulator are chosen at 0° , 15° , 30° respectively. Fig. 3.15 ~ Fig. 3.18 show the situations when MI=0.05, 0.1, 0.2 and 0.5 respectively.

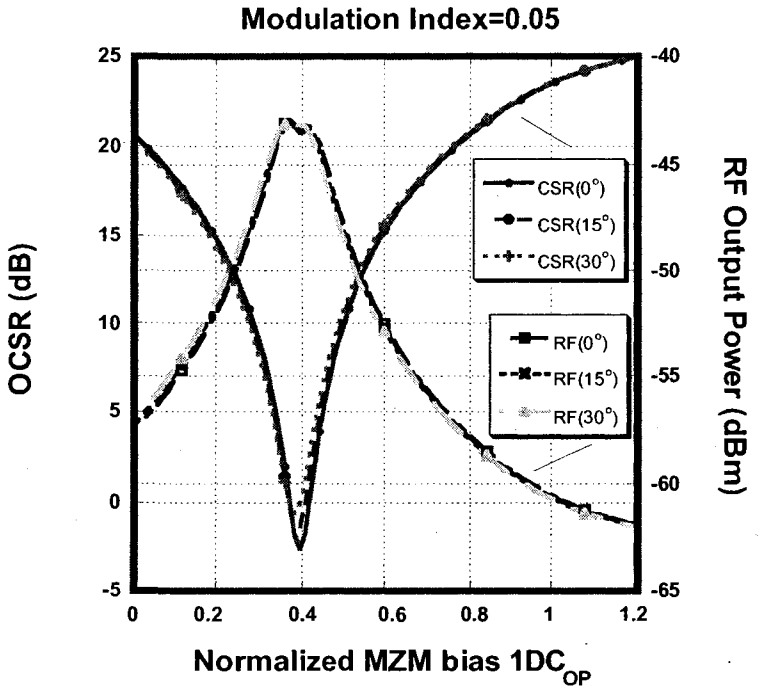

Fig. 3.15 Phase sensitivity when MI=0.05

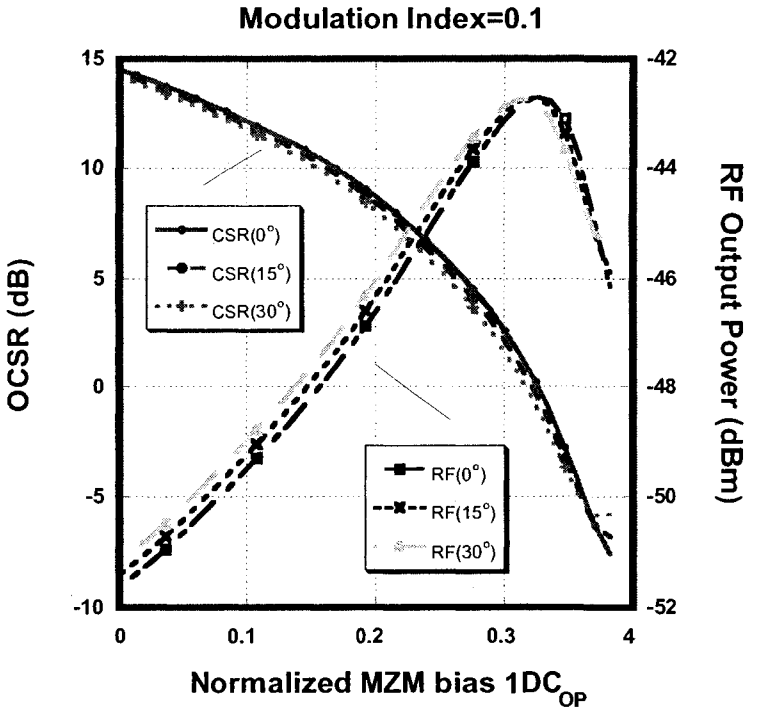

Fig. 3.16 Phase sensitivity when MI=0.1

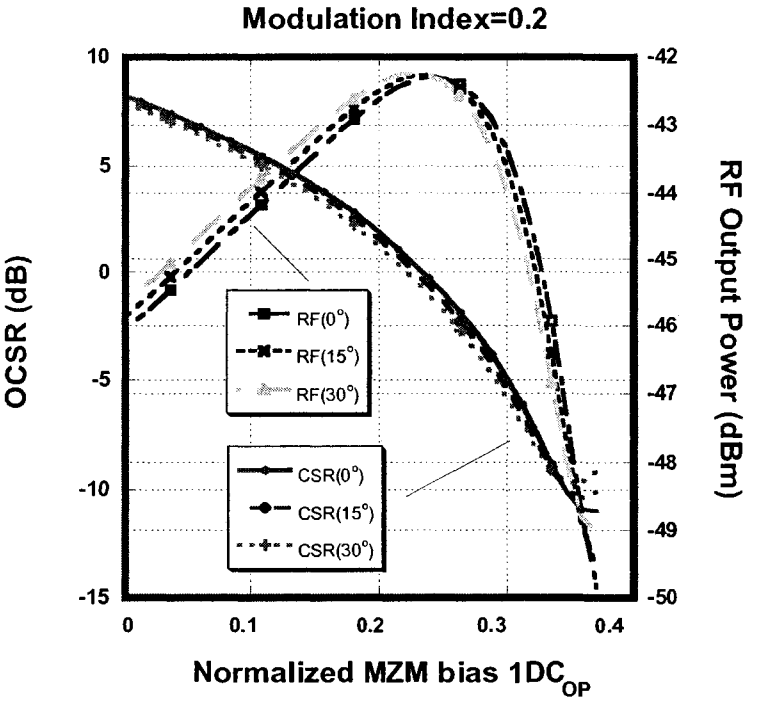

Fig. 3.17 Phase sensitivity when MI=0.2

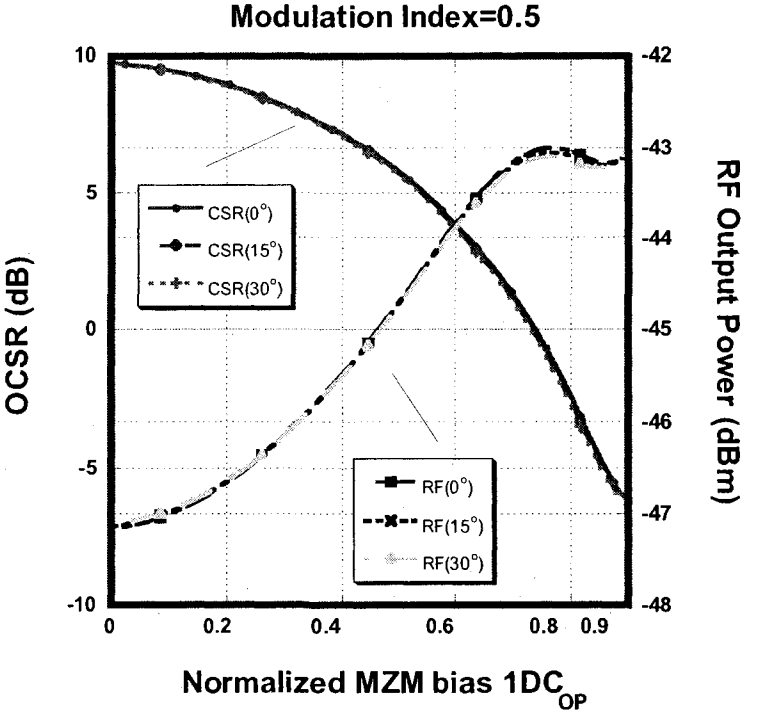

Fig. 3.18 Phase sensitivity when MI=0.1

All the figures display that the curves with different initial phase change very little and modulation efficiency using our proposed technique is not sensitive to the phase imbalance of the two parallel DE-MZMs.

3.2 Proposed modulator driven by two RF signals

In the previous section, we investigated how to optimize OCSR by adjusting DC_{OP} and how OCSR impacts the performance of system when only one RF signal is applied. However, the optimum OCSR has not been studied when two RF signals are applied. In the following, we investigate whether our modulation technique is effective to improve the performance of two RF signals system and whether the optimum OCSR to maximize the performance is still 0 dB.

As the theoretical analysis in Section 2.2.2, DC_{OP} influences OCSR the same way regardless one RF signal or two RF signals, which will be verified in the following section. Section 3.2.2 will describe how OCSR influences RF output power and IM3. In Section 3.2.3, we will investigate whether the frequency of RF signal will influence the system performance. In simulations of Sections 3.2.1 and 3.2.2, two RF signals at the frequencies of 5 GHz and 6 GHz are applied to our modulator.

3.2.1 Impact of $1DC_{OP}$ and $2DC_{OP}$ on OCSR

The meaning of optimizing OCSR was introduced in Section 3.1.2. For the adjustment of OCSR, the effect of sweeping $1DC_{OP}$ while keeping $2DC_{OP}$ fixed is equivalent to that of sweeping $2DC_{OP}$ while keeping $1DC_{OP}$ fixed. In the thesis, we sweep $1DC_{OP}$ and fix the normalized value of $2DC_{OP}$, ξ_2, at 1.06 for both extra small and small MIs, while ξ_2 is placed to 0 for medium MI. In the following figures, the results of theoretical analysis are also illustrated and compared with the simulation results.

Case 1 (MI=0.05): we sweep $1DC_{OP}$ from 0 V to 5V and the result is plotted in Fig. 3.19.

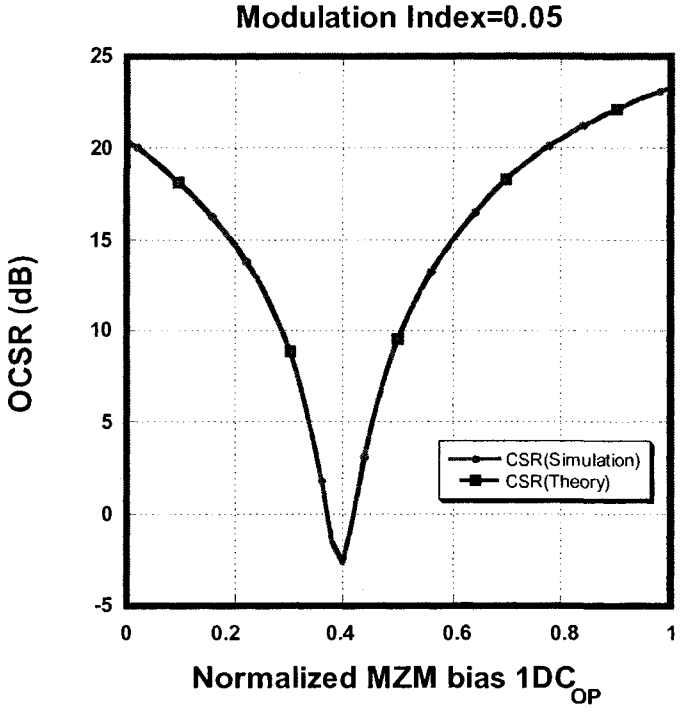

Fig. 3.19 Impact of $1DC_{OP}$ on OCSR when MI=0.05

In Fig. 3.19, OCSR decreases smoothly from 20.5 dB to 15 dB as we increase the value of ξ_1 from 0 to 0.2. While the value of ξ_1 is increased from 0.2 to 0.4, OCSR keeps decreasing until -2.7 dB and the slope of OCSR becomes sharper. After that, OCSR begins to increase swiftly and return to positive at the point of ξ_1=0.42. The curve of OCSR is symmetrical by the axis of ξ_1=0.4. In the interval between ξ_1=0.36 to ξ_1=0.42, the optical carrier is greatly suppressed that its power level is smaller than that of the sideband, which makes the value of OCSR be negative. Finally, the OCSR is decreased by 25.8 dB and the modulation efficiency is extremely improved.

Case 2 (MI=0.1): we sweep $1DC_{OP}$ from 0 V to 5V and the result is plotted in Fig. 3.20.

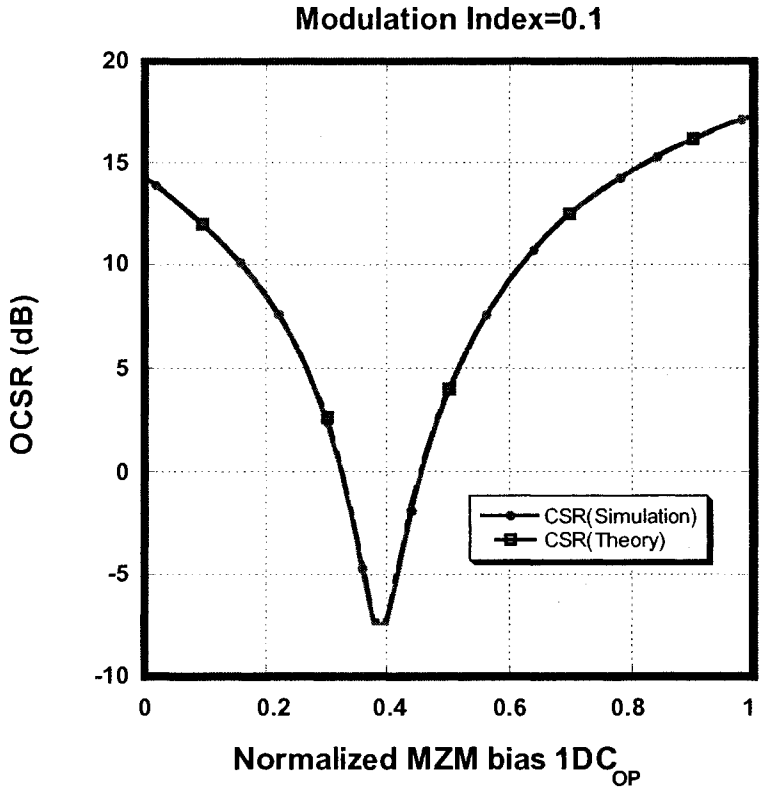

Fig. 3.20 Impact of $1DC_{OP}$ on OCSR when MI=0.1

In Fig. 3.20, OCSR decreases smoothly from 14.3 dB to 12 dB as we increase the value of ξ_1 from 0 to 0.2. While the value of ξ_1 is increased from 0.2 to 0.4, OCSR keeps decreasing until -7.4 dB and the slope of OCSR becomes sharper. After that, OCSR begins to increase swiftly and return to positive at the point of ξ_1=0.46. The curve of OCSR is symmetrical by the axis of ξ_1=0.39. In the interval between ξ_1=0.32 to ξ_1=0.46, the optical carrier is greatly suppressed that its power level is 7.4 dB smaller than that of the sideband, which makes the value of OCSR be negative. Finally, the OCSR is decreased by 24.9 dB and the modulation efficiency is extremely improved.

Case 3 (MI=0.2): we sweep $1DC_{OP}$ from 0 V to 5V and the result is plotted in Fig. 3.21.

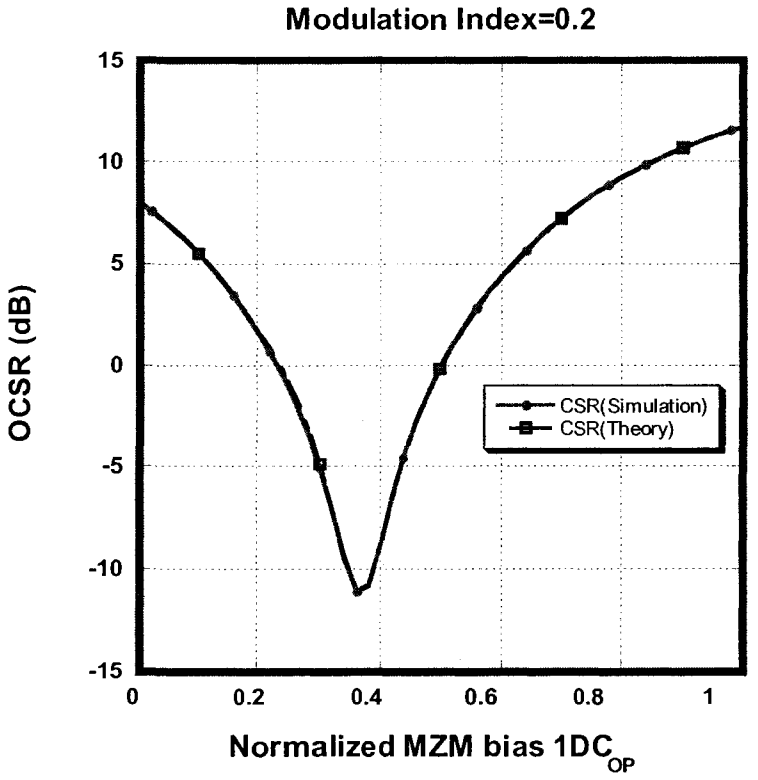

Fig. 3.21 Impact of $1DC_{OP}$ on OCSR when MI=0.2

In Fig. 3.21, OCSR decreases smoothly from 8.0 dB to 5.5 dB as we increase the value of ξ_1 from 0 to 0.1. While the value of ξ_1 is increased from 0.2 to 0.37, OCSR keeps decreasing until -11 dB and the slope of OCSR becomes sharper. After that, OCSR begins to increase swiftly and return to positive at the point of ξ_1=0.5. The curve of OCSR is symmetrical by the axis of ξ_1=0.37. In the interval between ξ_1=0.22 to ξ_1=0.5, the optical carrier is greatly suppressed that its power level is 11 dB smaller than that of the sideband, which makes the value of OCSR be negative. Finally, the OCSR is decreased by 22.7 dB and the modulation efficiency is extremely improved.

Case 4 (MI=0.5): we sweep $1DC_{OP}$ from 0 V to 5V and the result is plotted in Fig. 3.22.

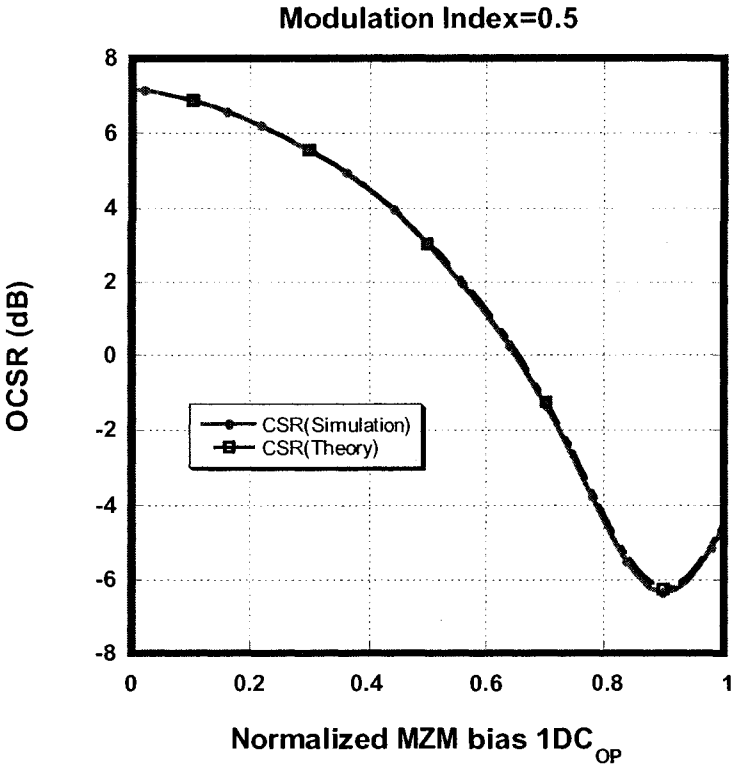

Fig. 3.22 Impact of $1DC_{OP}$ on OCSR when MI=0.5

In Fig. 3.22, OCSR decreases lightly from 7.2 dB to 4.5 dB as we increase the value of ξ_1 from 0 to 0.4. Then the curve decreases very quickly until -6.4 dB. After that, OCSR begins to increase swiftly. The optical carrier is greatly suppressed that its power level is 6.4 dB smaller than that of the sideband, which makes the value of OCSR be negative. Finally, the OCSR is decreased by 13.5 dB and the modulation efficiency is extremely improved.

Comparing Section 3.1.2 with Section 3.2.1, it is exceptionally apparent that ξ, ξ_1, and ξ_2 affect OCSR here the same way as in the case of one RF signal,

3.2.2 Impact of OCSR on RF output power and IM3

In this section, we investigate how OCSR impacts the performance of the system. We

choose three parameters as the criteria to evaluate the performance: RF output power, IM3 and SNR. In Section 2.2, theoretical analysis already proved that the power amplitudes of two RF outputs are equal to each other. In the following figures, the simulation results will be presented for the comparison with the theoretical analysis. Concerning IM3, this is the most harmful element of nonlinear distortion. Therefore, it is considerably necessary to study the change of IM3 caused by OCSR. Here, we define SNR as the subtraction between RF output power and IM3 power since other noise mechanisms are not considered. From Fig. 2.5, we can find that the $2f_1$-f_2 term is most detrimental for RF1 and the $2f_2$-f_1 term for RF2.

Case 1 (MI=0.05): we measure RF output powers, IM3s and SNRs and the results are shown in Fig. 3.23, Fig. 3.24 and Fig. 3.25.

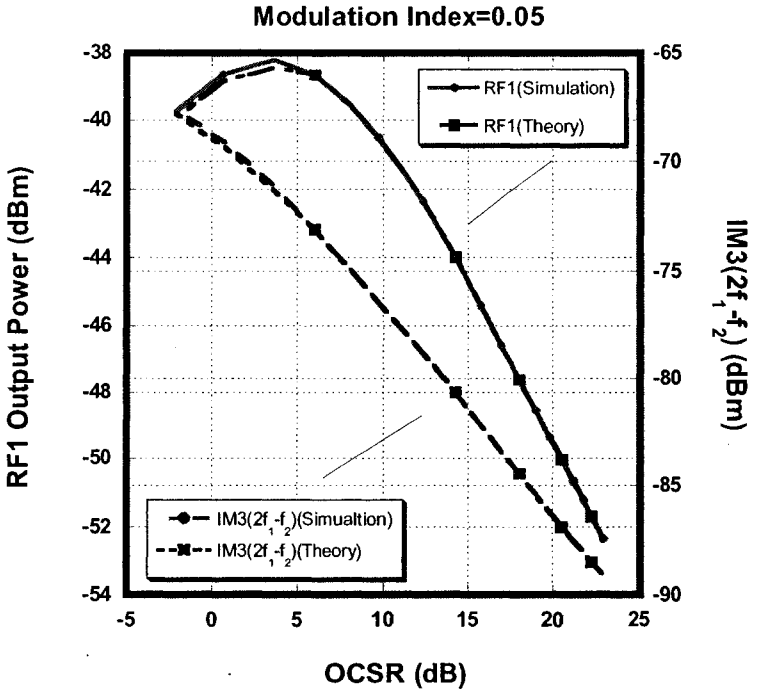

Fig. 3.23 Impact of OCSR on RF1 output power and IM3 ($2f_1$-f_2) when MI=0.05

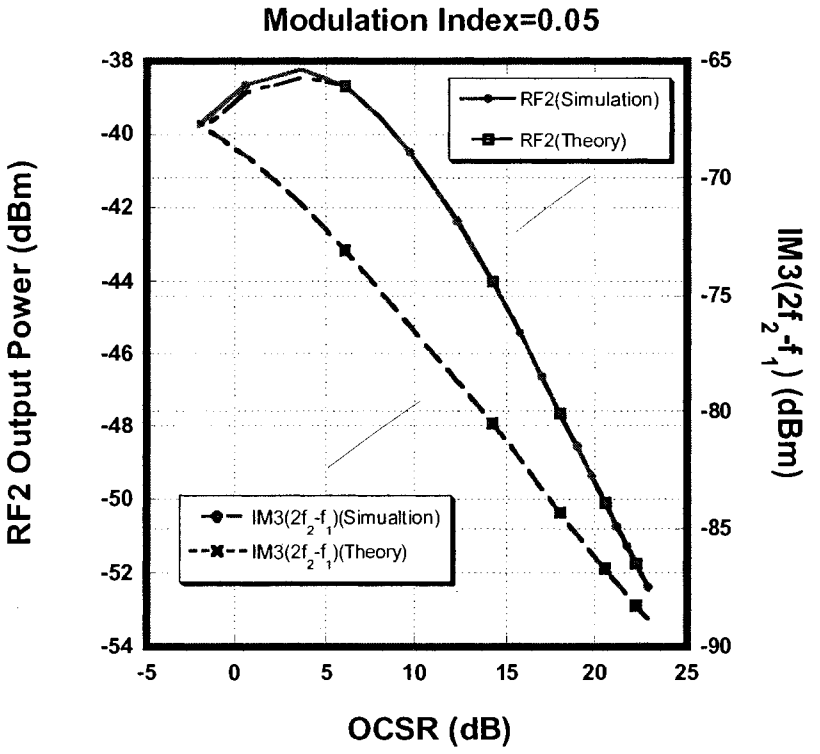

Fig. 3.24 Impact of OCSR on RF2 output power and IM3 ($2f_2$-f_1) when MI=0.05

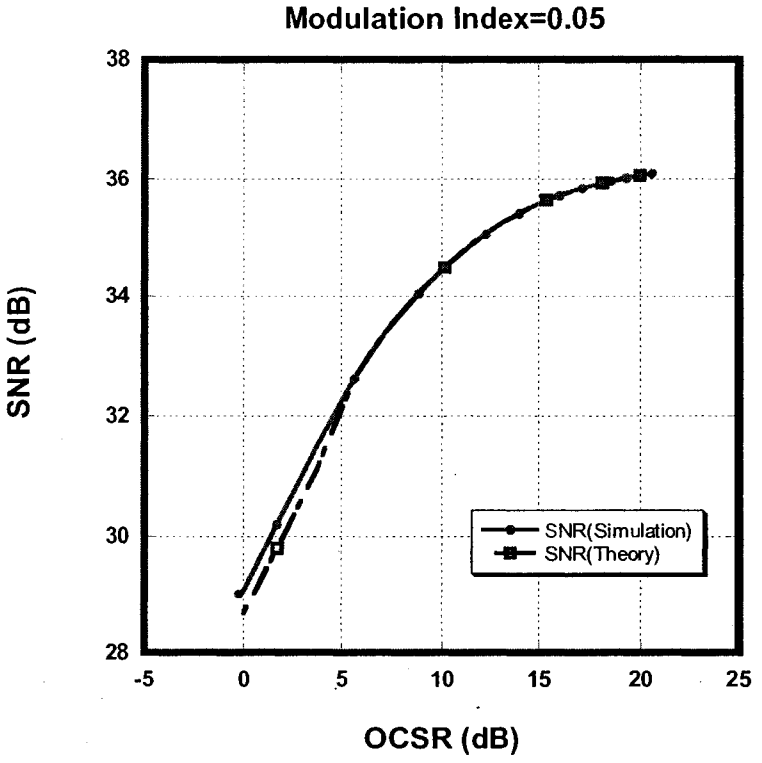

Fig. 3.25 Impact of OCSR on SNR when MI=0.05

In the above three figures, the curves from simulation results match very well with those from theoretical analysis and also RF1 output power in Fig. 3.23 is identical to RF2 output power in Fig. 3.24. As OCSR gets to decrease, the RF output powers keep increasing until OCSR=3 dB and start to decrease after that; The IM3 powers also keep increasing very quickly. Thus we can make a conclusion that RF output powers are maximized at OCSR=3 dB and IM3 arrives at the peak point at the most negative OCSR. From OCSR=21 dB to OCSR=3 dB, 14.5 dB improvements of RF output powers are achieved. In Fig. 3.25, as OCSR decreases from 21 dB, SNR decreases very slowly in the beginning but highly fast after, which is due to that at first IM3 increases slightly faster than RF output powers but much faster later.

Case 2 (MI=0.1): we measure RF output powers, IM3s and SNRs and the results are shown in plot Fig. 3.26, Fig. 3.27 and Fig. 3.28.

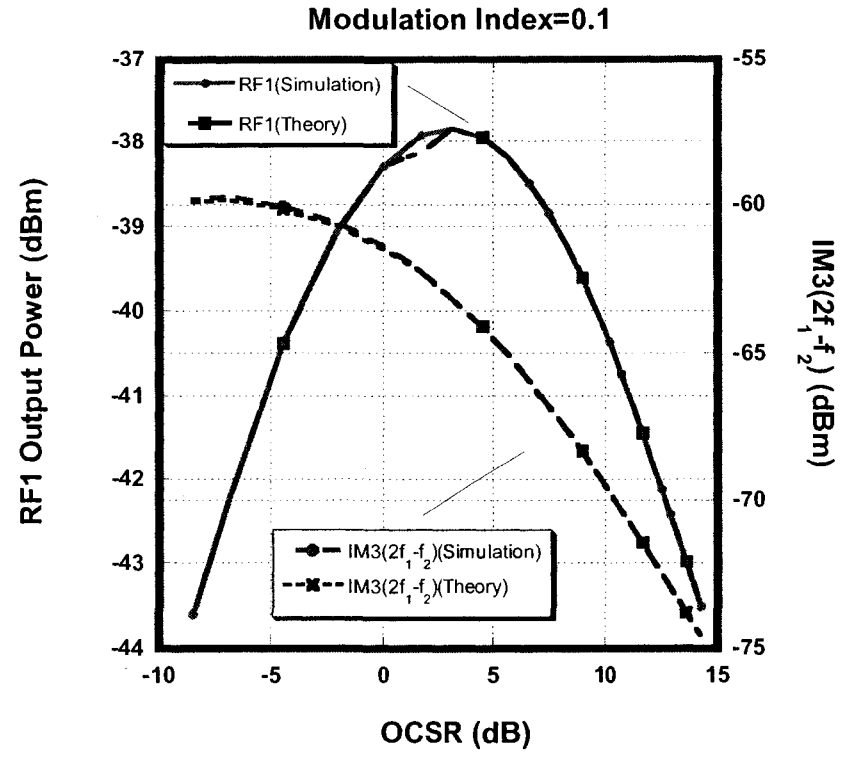

Fig. 3.26 Impact of OCSR on RF1 output power and IM3 ($2f_1$-f_2) when MI=0.1

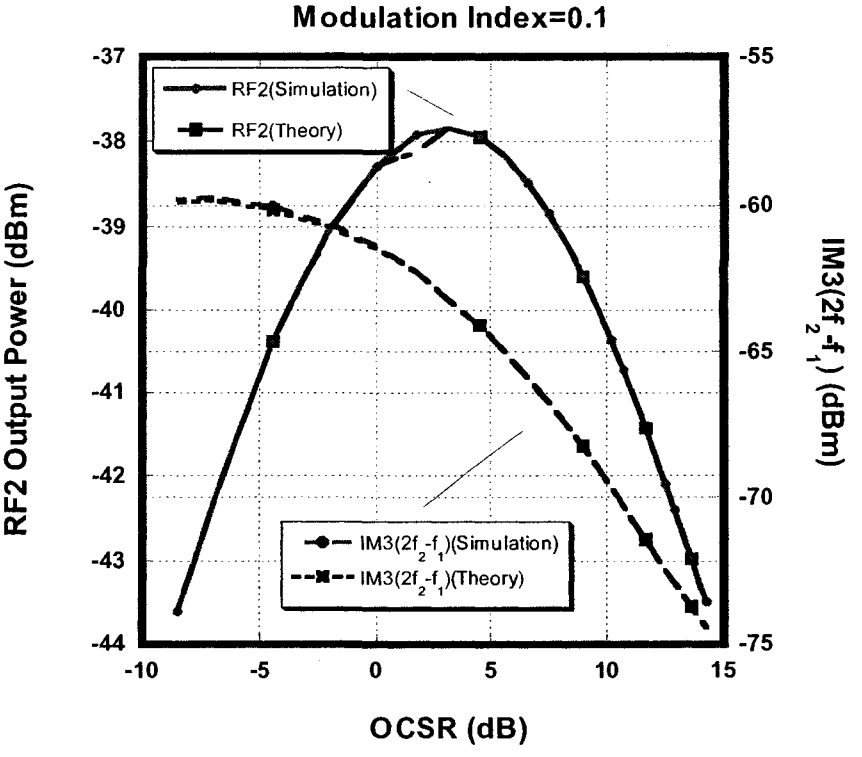

Fig. 3.27 Impact of OCSR on RF2 output power and IM3 ($2f_2$-f_1) when MI=0.1

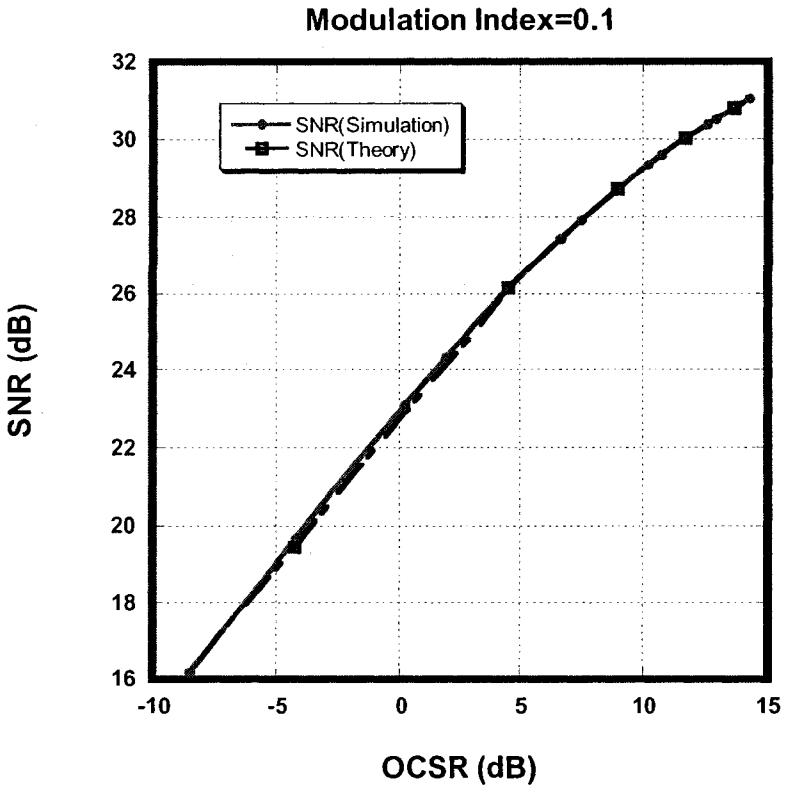

Fig. 3.28 Impact of OCSR on SNR when MI=0.1

In the above three figures, the curves from simulation results match very well with those from theoretical analysis and also RF1 output power in Fig. 3.26 is identical to RF2 output power in Fig. 3.27. As OCSR gets to decrease, the RF output powers keep increasing until OCSR=3 dB and start to decrease after that; the IM3 powers also keep increasing very quickly. Thus we can make a conclusion that RF output powers are maximized at OCSR=3 dB and IM3 arrives at the peak point at the most negative OCSR. From OCSR=14.4 dB to OCSR=3 dB, 6.4 dB improvements of RF output powers are achieved. In Fig. 3.28, as OCSR decreases from 14.4 dB, SNR decreases very slowly in the beginning but highly fast after, which is due to that at first IM3 increases slightly faster than RF output powers but much faster later.

Case 3 (MI=0.2): we measure RF output powers, IM3s and SNRs and the results are plotted in Fig. 3.29, Fig. 3.30 and Fig. 3.31.

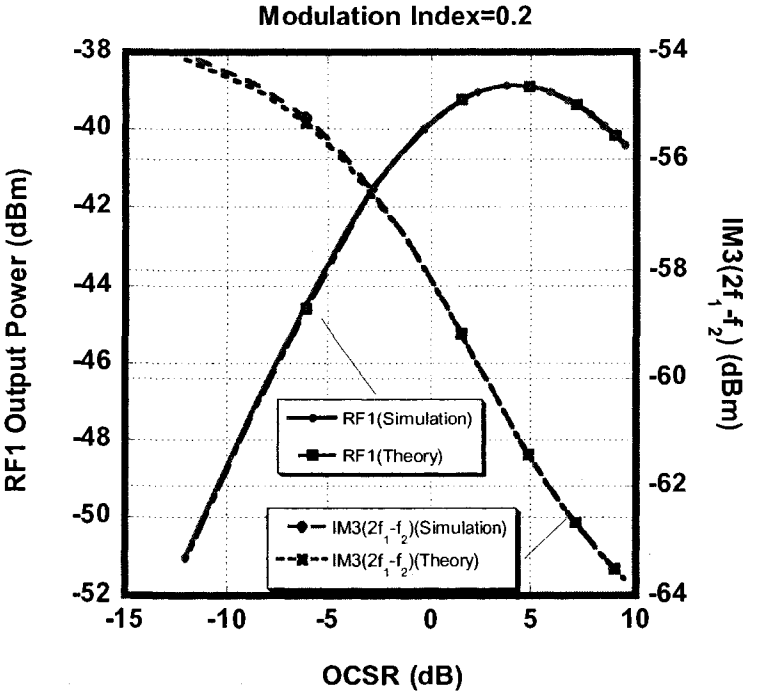

Fig. 3.29 Impact of OCSR on RF1 output power and IM3 ($2f_1$-f_2) when MI=0.2

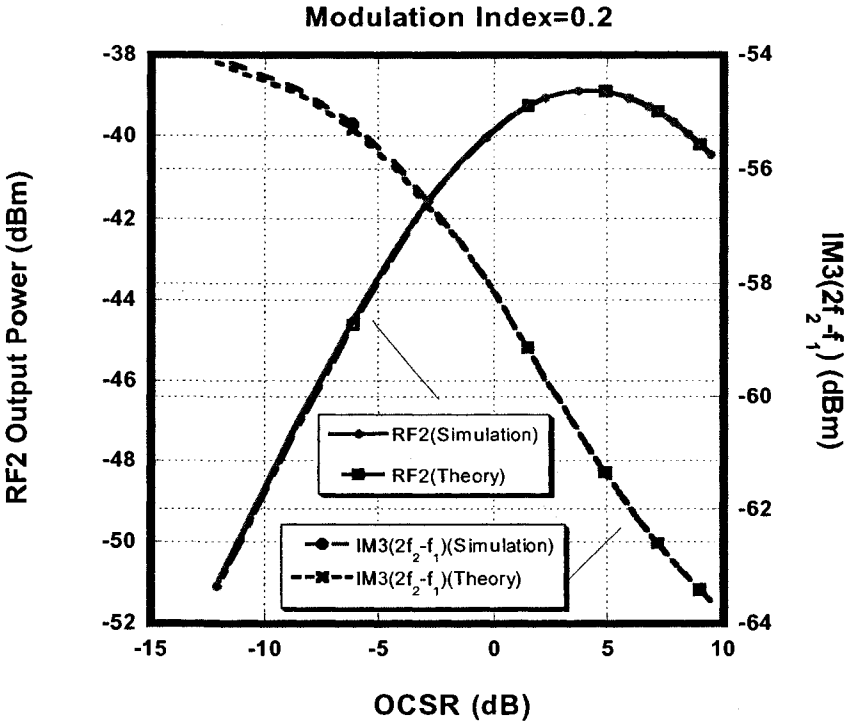

Fig. 3.30 Impact of OCSR on RF2 output power and IM3 ($2f_2$-f_1) when MI=0.2

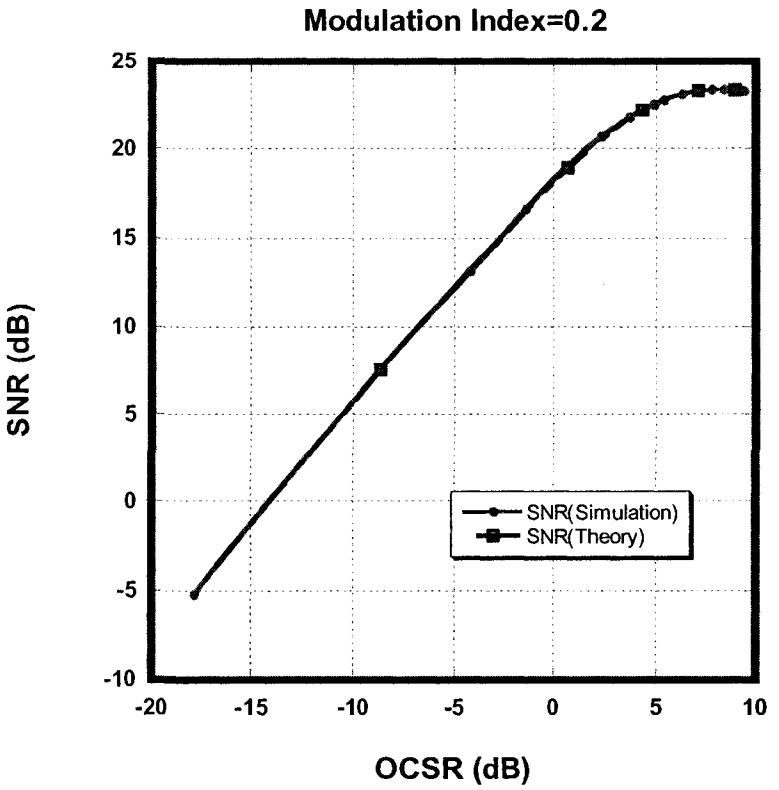

Fig. 3.31 Impact of OCSR on SNR when MI=0.2

In the above three figures, the curves from simulation results match very well with those from theoretical analysis and also RF1 output power in Fig. 3.29 is identical to RF2 output power in Fig. 3.30. As OCSR gets to decrease, the RF output powers keep increasing until OCSR=3 dB and start to decrease after that; the IM3 powers also keep increasing very quickly. Thus we can make a conclusion that RF output powers are maximized at OCSR=3 dB and IM3 arrives at the peak point at the most negative OCSR. From OCSR=9.5 dB to OCSR=3 dB, 2.4 dB improvements of RF output powers are achieved. In Fig. 3.31, as OCSR decreases from 9.5 dB, SNR decreases very slowly in the beginning but highly fast after, which is due to that at first IM3 increases slightly faster than RF output powers but much faster later.

Case 4 (MI=0.5): we measure RF output powers, IM3s and SNR and the results are shown in Fig. 3.32, Fig. 3.33 and Fig. 3.34.

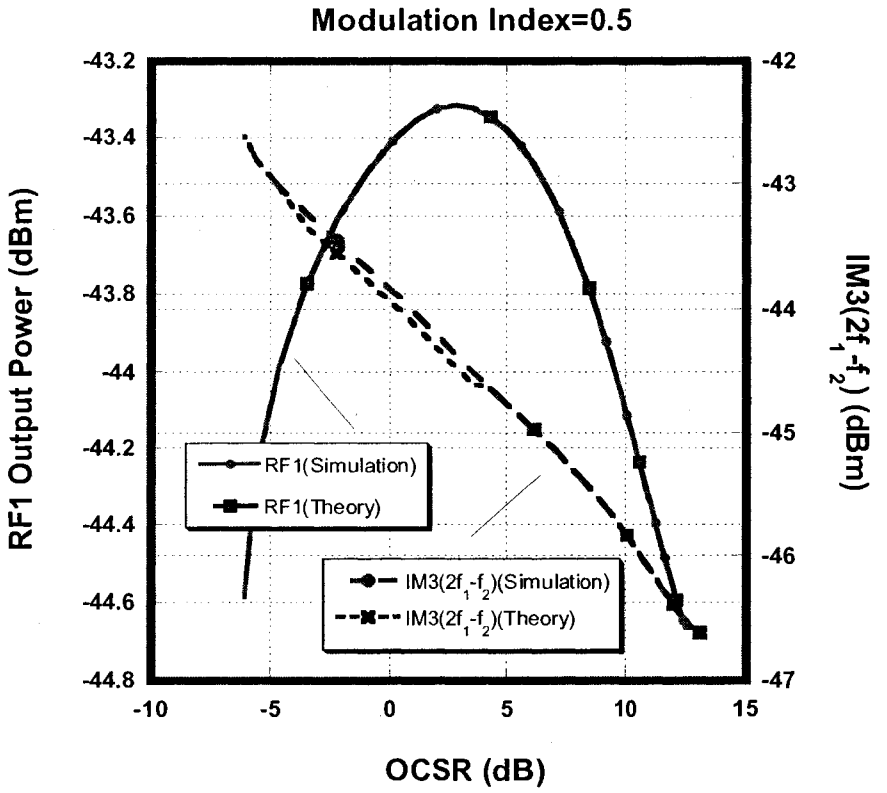

Fig. 3.32 Impact of OCSR on RF1 output power and IM3 ($2f_1$-f_2) when MI=0.5

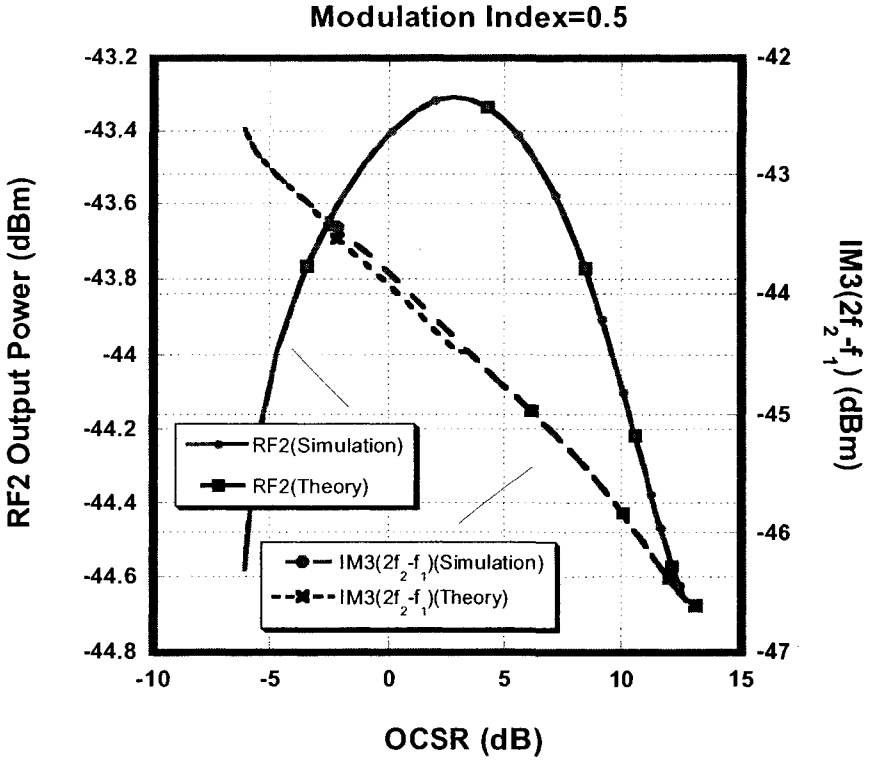

Fig. 3.33 Impact of OCSR on RF2 output power and IM3 ($2f_2$-f_1) when MI=0.5

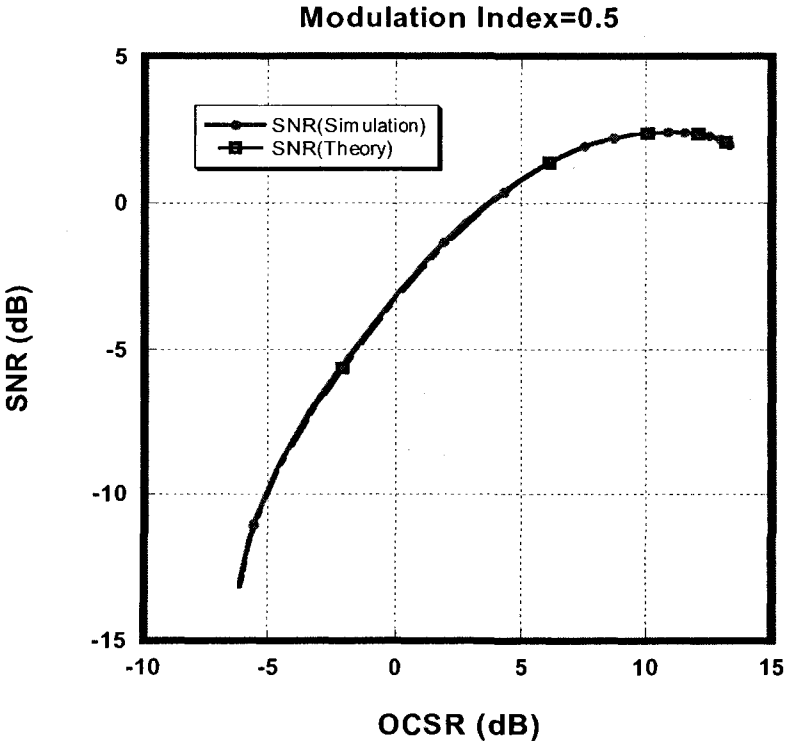

Fig. 3.34 Impact of OCSR on SNR when MI=0.5

In the above three figures, the curves from simulation results match very well with those from theoretical analysis and also Fig. 3.32 has the same shape with Fig. 3.33. As OCSR gets to decrease, the RF output powers keep increasing until OCSR=3 dB and start to decrease after that; the IM3 powers also keep increasing very quickly. Thus we can make a conclusion that RF output powers are maximized at OCSR=3 dB and IM3 arrives at the peak point at the most negative OCSR. From OCSR=13.2 dB to OCSR=3 dB, 1.3 dB improvements of RF output powers are achieved. In Fig. 3.31, as OCSR decreases from 13.2 dB, SNR decreases very slowly in the beginning but highly fast after, which is due to that at first IM3 increases slightly faster than RF output powers but much faster later.

All the curves of RF output powers show that their values reach the peak when OCSR= 3dB, *i.e.* the optimum OCSR. This optimum OCSR exists is due to the interplay among the optical power of optical carrier (P_{OC}), RF1 fundamental component (P_{O1}), and RF2 fundamental component (P_{O2}). From the discussion above, we know P_{O1} is equal to P_{O2}. The sum of P_{OC}, P_{O1} and P_{O2} is a constant when the output power of EDFA is fixed as C. The electrical output power of RF1 (P_{E1}) is proportional to the optical-power product of the optical carrier and its fundamental component, *i.e.*, $P_{E1} \propto \sqrt{P_{OC}P_{O1}} \approx \sqrt{(C-2P_{O1})P_{O1}}$. In the cases of extra small MI and small MI, the expression above is extremely accurate because HDs and IMDs are negligible compared with P_{OC}, P_{O1}, and P_{O2}. From the expression, we conclude that P_{E1} achieves the maximum value only when $P_{OC}=2P_{O1}=C/2$, *i.e.* OCSR=3 dB. The mechanism can leads to 14.5 dB, 6.4 dB, 2.4 dB and 1.3 dB

improvements of RF output powers when MI=0.05, 0.1, 0.2 and 0.5 respectively. Our proposed modulation technique is still more efficient in small MI cases than in large MI cases. That's because in small MI cases, the initial OCSR is large and can be improved enormously. Furthermore, HDs and IMDs are much smaller than those in medium and large MI cases. When nonlinear distortions increase tremendously, considerable portion of pump energy from EDFA will be consumed by them, which decreases the efficiency of our modulation technique greatly.

IM3 is another important parameter to evaluate the system performance. From the figures above, IM3 keeps increasing quickly as OCSR decreases. As can be seen in Fig. 3-25, Fig. 3-28, Fig. 3-31 and Fig. 3-34, SNR decreases slowly at first as OCSR decreases and decrease swiftly when OCSR is below 3 dB. The reason why SNR decreases as OCSR decreases is that IM3 always increases faster than RF output powers. When OCSR is below 3 dB, RF output powers begins to decrease but IM3 still continues to increase, which leads to that SNR decrease faster.

Why SNR keeps decreasing is explained mathematically. P_{OC}, P_{RF} and P_{IM3} represent the optical powers of optical carrier, fundamental RF sideband and IM3 component respectively before EDFA. Once MI is fixed, the subtraction between P_{RF} and P_{IM3} becomes a constant and we define that as C_1. Another constant C_2 represents the fixed output power of EDFA. Then we obtain

$$P_{OC} = P_{RF} + OCSR$$
$$P_{RF} - P_{IM3} = C_1$$

If we define G as the optical gain from EDFA, we can express SNR as

$$SNR = G(P_{RF} - P_{IM3})P_{OC} = C_1 G(P_{RF} + OCSR)$$

$$G = \frac{C_2}{P_{OC} + P_{RF} + P_{IM3}} = \frac{C_2}{3P_{RF} + OCSR - C_1}$$

Finally, we combine them together and get

$$SNR = \frac{C_1 C_2 (P_{RF} + OCSR)}{3P_{RF} + OCSR - C_1} = \frac{C_1 C_2}{1 + \frac{2P_{RF} - C_1}{P_{RF} + OCSR}}$$

It is concluded that SNR decreases when OCSR decreases.

3.2.3 Impact of frequencies of RF signals on SNR

The conclusion from the previous section states SNR decreases as OCSR decreases. In this section, we investigate whether the frequencies of RF signals have an influence on system performance. Two sets of simulations in which f_2-f_1 is equal to 1 GHz and 2 GHz respectively are shown in Fig. 3.35 and Fig. 3.36. In each set, we sweep the frequencies of RF signal when OCSR=0 dB, 10 dB and 20 dB respectively and the results are plotted in Fig. 3.35 and Fig. 3.36. SNR_1 is defined as the electrical power subtraction between RF1 output and $2f_1$-f_2 term while SNR_2 is the electrical power subtraction between RF2 output and $2f_2$-f_1 term.

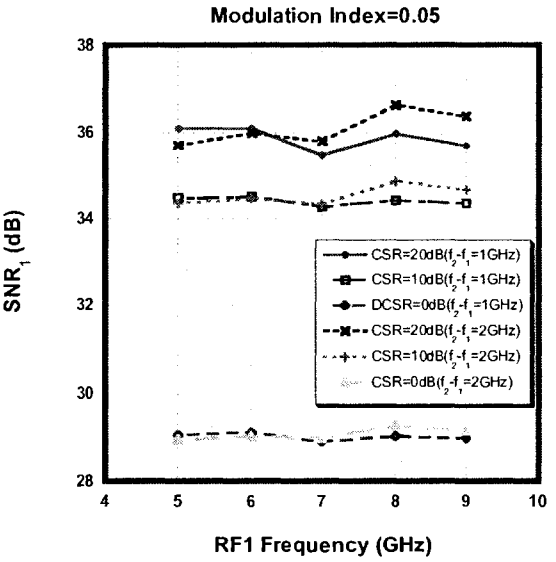

Fig. 3.35 Impact of RF1 frequency on SNR_1

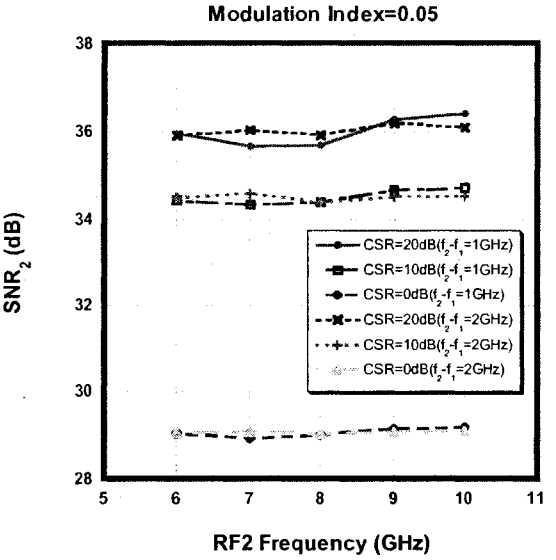

Fig. 3.36 Impact of RF2 frequency on SNR_2

Fig. 3.35 and Fig. 3.36 show the frequencies of RF signals have little influence on SNR. Regardless what frequencies are employed, SNR will not be improved or degraded. In the future work, we will change the ideal connection between EDFA and PD into standard single mode fiber. In that case, the situation will be different and the frequencies of RF signals will have great impact on SNR.

When two RF signals are applied to modulate optical carrier by our technique, RF output powers will be greatly improved but SNR won't. However, several explanations are made as follows:

1. If we use our proposed modulation technique and keep modulation index the same, RF output power can be greatly improved and SNR will be degraded by a little degree. To some extent, it plays the role like an amplifier. When signal goes through an amplifier, its power will be increased but its SNR will also be slightly degraded. In addition, compared to the weakly modulated OSSB SCM, although SNR is slightly degraded, our technique can maximize the RF output power and make the RoF system more robust to other noise interference.

2. In order to obtain identical RF output power, small MI modulation can be applied by using our proposed modulation technique while large MI modulation should be applied by employing typical OSSB SCM. In that case, SNR using our proposed modulation technique is still larger that in typical OSSB SCM. For instance, the RF output power is -53dBm when modulation index is equal to 0.05 in typical OSSB SCM. In order to obtain higher RF output power i.e. -43dBm, we have two ways. One is still using typical OSSB SCM and increasing modulation index to improve modulation efficiency. In that case, 0.12 should be chosen for ξ and the corresponding SNR is 29.8dB. The other is choosing our proposed modulation technique and improving modulation efficiency by adjusting DC_{OP}. The corresponding SNR is 35.3dB. In all, a great improvement of SNR can be achieved.

3. When paying attention to the range of SNR degradation, we find from the largest OCSR to the optimum OCSR the SNR degradations are 4 dB, 5 dB, 1 dB and 3 dB respectively, which is not large.

4. Although IM3 is highly detrimental to system performance, it is possible to suppress or even avoid it by choosing frequencies of RF signals properly. If we enlarge the frequency difference between RF signals, IM3 may be avoided completely. For instance, IM3 can be handily filtered out by appropriate electrical filters when the frequencies of RF1 and RF2 are 7 GHz and 10 GHz respectively.

Chapter 4 Conclusions and future work

4.1 Major contribution

In this thesis, a novel modulation technique using two parallel Mach-Zehnder modulators for radio over fiber systems is proposed and then theoretical analysis is presented. With such a modulator, we can obtain optical single sideband SCM and adjustable optical carrier-to-sideband ratio. Two cases are considered: one RF signal and two RF signals driving the proposed modulator, respectively. The theoretical analysis is finally verified by computer simulations.

By both theoretical analysis and simulation, it is shown that our proposed modulation technique can provide optical single sideband SCM and adjustable optical carrier-to-sideband ratio. When one RF signal is applied to modulate an optical carrier, modulation efficiency can be improved and be able to improve RF output power and SNR considerably, and the optimized optical carrier-to-sideband ratio is found 0 dB. However, the improved performance is limited by nonlinear distortion for large modulation indexes. When two RF signals are employed to modulate an optical carrier, RF output power increases with the decrease of optical carrier-sideband ratio, but IM3 power also increases and the increase rate is faster than RF output power. Thus, SNR decreases as optical carrier-sideband ratio decreases. At optical carrier-to-sideband ratio of 3 dB, RF output powers are maximized, rather than 0 dB for the case of one RF signal. For both cases, the improvement using our proposed modulation technique is higher in

small modulation index cases than that in large modulation index cases.

The advantage of proposed novel modulation technique is that we do not need any additional optical or electrical components after modulator to realize an optical carrier suppressed OSSB. Compared with other methods of suppressing optical carrier, this proposed modulation technique is simple, stable and easy to implement. Without bringing any distortions or other detrimental terms, this proposed modulation technique can improve the performance of RoF systems greatly.

4.2 Future work

In this work, some conditions are considered ideally in computer simulations. The laser source, EDFA and PD are supposed to be noise free. The connection between EDFA and PD is applied also ideally in all simulations except in Section 3.1.1. As we know, if we use standard single mode optic fiber, chromatic terms should be added into analytical model and the results will be different in computer simulation. Besides, only analogue RF signal is considered here to transmit over the link. However, those digital data formats *e.g.* DPSK, QPSK and QAM are also commonly utilized to transmit in RoF systems. Therefore, we will focus on the situation when different type of signal is transmitted.

References

[1] H Ogawa, D Polifko and S Banba, "Millimeter-wave fiber optical systems for personal radio communication," *IEEE Trans. on Microwave Theory and Technique*, vol. 40, No. 12, pp.2294-2302, Dec. 1992.

[2] D. Wake, D. Johansson and D. Moodie, "Passive Pico-cell: a new concept in wireless network infrastructure," *Electron. Lett.*, vol.33, pp.404-406, Feb. 1997.

[3] D. Wake, "Radio over Fiber Systems for Mobile Applications" in *Radio over Fiber Technologies for Mobile Communications Networks*, H, Al-Raweshidy, and S. Komaki, ed. (Artech House, Inc, USA, 2002).

[4] D. Wake, and K. Beachman, "A Novel Switched Fiber Distributed Antenna System", in *Proceedings of European Conference on Optical Communications (ECOC'04)*, Vol. 5, 2004, pp. 132 – 135.

[5] J. Capmany, B. Ortega, D. Pastor, and S. Sales, "Discrete-Time Optical Processing of Microwave Signals", *JLT*, Vol. 23, No. 2, 703 - 723, (2005).

[6] G. Maury, A. Hilt, T. Berceli, B. Cabon, and A. Vilcot, "Microwave Frequency Conversion Methods by Optical Interferometer and Photodiode", *IEEE Trans. On Microwave Theory and Techniques*, Vol. 45, No. 8, 1481 - 1485, (1997).

[7] D. Wake, S. Dupont, J-P. Vilcot, A. J. Seeds, "32-QAM Radio Transmission Over Multimode Fiber Beyond the Fiber Bandwidth", in *Proceedings of the IEEE International Topical Meeting on Microwave Photonics (MWP'01), 2001.*

[8] D. Wake, S. Dupont, C. Lethien, J-P. Vilcot, and D. Decoster, "Radiofrequency Transmission over Multimode Fiber for Distributed Antenna System Applications", *Electronic Letters*, Vol. 37, No. 17, pp 1087 – 1089 (2001).

[9] C. Liu, A. Seeds, J. Chadha, P. Stavrinou, G. Parry, M. Whitehead, A. Krysa, and J. Roberts, "Bi-Directional Transmission of Broadband 5.2 GHz Wireless Signals Over Fiber Using a Multiple-Quantum-Well Asymmetric Fabry-Perot Modulator/Photo detector", in *Proceedings of the Optical Fiber Communications (OFC) Conference.* 2003, Vol. 2, pp. 738 – 740.

[10] H. Al-Raweshidy, S. Komaki, ed., "Radio over Fiber Technology for the Next Generation" in *Radio over Fiber Technologies for Mobile Communications Networks*, (Artech House, Inc, USA, 2002).

[11] U. Gliese, T. N. Nielsen, S. Norskov, and K.E. Stubkjaer, "Multifunction Fiber-Optic Microwave Links Based on Remote Heterodyne Detection", *IEEE Trans. On Microwave Theory and Techniques*, vol. 46, No. 5, 458-468, (1998)

[12] G. J. Meslener, "Chromatic dispersion induced distortion of modulated monochromatic light employing direct detection," *IEEE J. Quantum Electron.*, vol. QE-20, no. 10, pp. 1208–1216, Oct. 1984.

[13] H. Schmuck, "Comparison of optical millimeter-wave system concepts with regard to chromatic dispersion," *Electronic Letters*, vol. 31, no. 21, pp. 1848–1849, Oct. 1995.

[14] U. Gliese, S. Norskov, and T. N. Nielsen, "Chromatic dispersion in fiber-optic

microwave and millimeter-wave links," *IEEE Trans. Microwave. Theory Tech.*, vol. 44, no. 10, pp. 1716–1724, Oct. 1996.

[15] G. H. Smith, D. Novak, and Z. Ahmed, "Technique for optical SSB generation to overcome dispersion penalties in fiber-radio systems," *Electronic Letters*, vol. 33, no. 1, pp. 74–75, Jan. 1997.

[16] J. Park, W. V. Sorin, and K. Y. Lau, "Elimination of the fiber chromatic dispersion penalty on 1550 nm millimeter-wave optical transmission," *Electronic Letters*, vol. 33, no. 6, pp. 512–513, Mar. 1997.

[17] E.Vergnol, D. Tanguy, J. F. Cadiou, A. Carenco, and E. Penard, "Multicarrier and m-QAM modulation based on integrated single side band lightwave source," in *Proc. Opt. Fiber Commun. Conf., San Diego, CA*, Feb. 1999, pp. 224–226.

[18] E. Vourch, D. Le Berre, and D. Herve, "Lightwave single sideband wavelength self-tunable filter using InP: Fe crystal for fiber-wireless systems," *IEEE Photon. Technol. Lett.*, vol. 14, no. 2, pp. 194–196, Feb. 2002.

[19] R. D. Esman and K. J. Willians, "Wideband efficiency improvement of fiber optic systems by carrier subtraction," *IEEE Photon. Technol. Lett.*, vol. 7, no. 2, pp. 218–220, Feb. 1995.

[20] M. J. LaGasse, W. Charczenko, M. C. Hamilton, and S. Thaniyavarn, "Optical carrier filtering for high dynamic range fiber optic links," *Electronic Letters*, vol. 30, no. 25, pp. 2157–2158, Dec. 1994.

[21] Christina Lim, Manik Attygalle etc., "Analysis of Optical Carrier-to-Sideband Ratio

for Improving Transmission Performance in Fiber-Radio Links", *IEEE Transactions on Microwave Theory and Techniques*, vol.54 No.5, May 2006, pp.2181-2187.

[22] S. Tonda-Goldstein, D. Dolfi, J-P. Huignard, G. Charlet, and J. Chazelas, "Stimulated brillouin scattering for microwave signal modulation depth increase in optical links," *Electronic Letters*, vol. 36, no. 11, pp. 944–946, May 2000.

[23] H. Toda, T. Yamashita, T. Kuri, and K. Kitayama, "25-GHz channel spacing DWDM multiplexing using an arrayed waveguide grating for 60-GHz band radio-on-fiber systems," in *Proc. Microw. Photon.*, Budapest, Hungary, Sep. 2003, pp. 287–290.

[24] W. W. Hu, K. Inagaki, T. Tanaka, T. Ohira and A. Xu, "High SNR 50 GHz radio-over-fiber uplink system by use of low biased Mach-Zehnder modulator technique", *Electronic Letters*, 27th April 2006, vol. 42 No. 9.